Available online at www.sciencedirect.com
ScienceDirect
Renewable and Sustainable Energy Reviews
12 (2008) 593–661
RENEWABLE & SUSTAINABLE ENERGY REVIEWS
www.elsevier.com/locate/rser

A key review on exergetic analysis and assessment of renewable energy resources for a sustainable future

Arif Hepbasli*

Department of Mechanical Engineering, Faculty of Engineering, Ege University, TR-35100 Bornova, Izmir, Turkey

Received 2 August 2006; accepted 13 October 2006

Abstract

Energy resources and their utilization intimately relate to sustainable development. In attaining sustainable development, increasing the energy efficiencies of processes utilizing sustainable energy resources plays an important role. The utilization of renewable energy offers a wide range of exceptional benefits. There is also a link between exergy and sustainable development. A sustainable energy system may be regarded as a cost-efficient, reliable, and environmentally friendly energy system that effectively utilizes local resources and networks. Exergy analysis has been widely used in the design, simulation and performance evaluation of energy systems.

The present study comprehensively reviews exergetic analysis and performance evaluation of a wide range of renewable energy resources (RERs) for the first time to the best of the author's knowledge. In this regard, general relations (i.e., energy, exergy, entropy and exergy balance equations along with exergy efficiency, exergetic improvement potential rate and some thermodynamic parameters, such as fuel depletion ratio, relative irreversibility, productivity lack and exergetic factor) used in the analysis are presented first. Next, exergetically analyzed and evaluated RERs include (a) solar energy systems; (a1) solar collector applications such as solar water heating systems, solar space heating and cooling, solar refrigeration, solar cookers, industrial process heat, solar desalination systems and solar thermal power plants), (a2) photovoltaics (PVs) and (a3) hybrid (PV/thermal) solar collectors, (b) wind energy systems, (c) geothermal energy systems, (c1) direct utilization (district heating, geothermal or ground-source heat pumps, greenhouses and drying) and (c2) indirect utilization (geothermal power plants), (d) biomass, (e) other renewable energy systems, and (f) country based RERs. Studies conducted on these RERs are then compared with the previously ones in tabulated forms, while the Grassmann (or exergy flow) diagrams, which are a very

Abbreviations: GDHS, geothermal district heating system; GSHP, ground source heat pump; RE, renewable energy; RER, renewable energy resource; SPC, solar parabolic cooker

*Tel.: +90 232 343 4000x5124; fax: +90 232 388 8562.
E-mail addresses: arif.hepbasli@ege.edu.tr, hepbasli@egenet.com.tr.

1364-0321/$ - see front matter © 2006 Elsevier Ltd. All rights reserved.
doi:10.1016/j.rser.2006.10.001

useful representation of exergy flows and losses, for some RERs are given. Finally, the conclusions are presented. It is expected that this comprehensive study will be very beneficial to everyone involved or interested in the exergetic design, simulation, analysis and performance assessment of RERs.
© 2006 Elsevier Ltd. All rights reserved.

Keywords: Analysis; Biomass; Drying; Efficiency; Exergy; Geothermal; Geothermal power plants; Heat pumps; Hybrid systems; Photovoltaic; Renewable energy; Solar; Sustainability; Wind

Contents

1. Introduction

Achieving solution to environmental problems that we face today requires long-term potential actions for sustainable development. In this regard, renewable energy resources (RERs) appear to be the one of the most efficient and effective solutions [1].

RERs (i.e., solar, hydroelectric, biomass, wind, ocean and geothermal energy) are inexhaustible and offer many environmental benefits compared to conventional energy sources. Each type of renewable energy (RE) also has its own special advantages that make it uniquely suited to certain applications. Almost none of them release gaseous or liquid

Nomenclature

a	amplitude, share of renewables in the total of each component
A	area (m^2)
C	specific heat (kJ/kg K)
COP	coefficient of performance (dimensionless)
$\dot{E}$	energy rate (kW)
ex	specific exergy (kJ/kg)
$\dot{\mathrm{E}}\mathrm{x}$	exergy rate (kW)
f	exergetic factor, the sunlight dilution factor (dimensionless)
$\dot{F}$	exergy rate of fuel (kW)
g	gravitational constant (m/s^2)
h	specific enthalpy (kJ/kg)
HV	heating value (kJ/kg)
HHV	higher heating (gross calorific) value (kJ/kg)
I	global irradiance (W/m^2)
$\dot{I}$	rate of irreversibility, rate of exergy consumption (kW)
$\mathrm{I}\dot{\mathrm{P}}$	rate of improvement potential (kW)
L	enthalpy of phase change (kJ/kg)
LHV	lower heating (net calorific) value (kJ/kg)
$\dot{m}$	mass flow rate (kg/s)
n	number, index number (dimensionless)
P	pressure (kPa)
$\dot{P}$	exergy rate of the product (kW)
$\dot{Q}$	heat transfer rate (kW)
r	renewable use by the residential–commercial sector in energy terms (kJ)
R	ideal gas constant (kJ/kgK)
s	specific entropy (kJ/kgK)
$\dot{S}$	entropy rate (kW/K)
SExI	specific exergy index (dimensionless)
t	period between local maxima and minima of the tidal record, time (s)
T	temperature (°C or K)
U	heat transfer coefficient ($kW/m^2 K$)
V	speed (m/s)
W	work (kJ)
$\dot{W}$	rate of work (or power) (kW)
y	mol fraction (dimensionless)
z	vertical distance from the water level of the reservoir to the reference height or average sea level (m)
Z	mass fraction (dimensionless)

Greek letters

σ	Stefan–Boltzmann constant ($W/m^2 K^4$)
κ	dilution factor (dimensionless)
η	energy (first law) efficiency (dimensionless)

Ψ	flow (specific) exergy (kJ/kg), maximum efficiency ratio (or exergy-to-energy ratio for radiation (dimensionless)
Δ	interval
ρ	density (kg/m^3)
β	proportionality constant (or quality factor or exergy coefficient)
δ	fuel depletion rate (dimensionless)
ε	exergy (second law) efficiency (dimensionless)
ξ	productivity lack (dimensionless)
χ	relative irreversibility (dimensionless)
ω	specific humidity ratio (kg_{water}/kg_{air})

Indices

a	air, actual
absor	absorber
adsor	adsorbent
am	ambient
at	atmospheric
ava	available
ave	average
be	beam
C	Carnot
c	cooking
ce	collector-evaporator
CH	chemical
col	collector
com	compressor
cond	condenser
conver	conversion
cook	cooker
cool	cooling
d	natural direct discharge, diffuse
da	drying air
dest	destroyed, destruction
diff	diffusive
e	electrical, evaporator
eff	effective
eng	engine
evap	evaporator
ex	exergetic
exrc	exergetic residential commercial
f	fuel
fc	fan-coil
fg	vaporization
g	generator
GDHS	geothermal district heating system
gen	generation, generated

gh	ground heat exchanger
h	heating, heat
HE	heat exchanger
HHV	higher heating value
HP	heat pump
HV	heating value
i	successive number of elements
ic	incompressible
in	input
io	inverter output
k	location
KN	kinetic
LHV	lower heating value
max	maximum
mech	mechanical
mix	mixture
o	overall
oe	overall electricity
of	overall fuel
or	overall residential
out	output
p	constant pressure, pump
par	parabolic
per	perfect
PH	physical
pot	potential
pp	power plant
pre	precipitation
PT	potential
PV	photovoltaic
Q	heat
r	reinjected thermal water, refrigerant
R	rational
Ran	Rankine
rc	residential-commercial
rec	receiver
res	reservoir
ro	residential overall
s	solar
scol	solar collector
sh	space heating
srad	solar radiation
sys	system
T	total, thermal
TEG	thermal gradient
trans	transformation
u	useful

v	water vapor
w	water
wa	water/antifreeze solution
wh	wellhead, water heating
wor	without reinjected thermal water
wr	with reinjected thermal water
0	dead (reference) state
1	initial state
2	final state

pollutants during operation. In their technological development, the renewable ranges from technologies that are well established and mature to those that need further research and development [1,2].

Even though conventional sources, such as oil, natural gas and coal meet most of the energy demand at the moment, the role of RERs and their current advances have to take more relevance in order to contribute to energy supply and support the energy conservation (or efficiency) strategy by establishing energy management systems [3]. The use of RE offers a range of exceptional benefits, including: a decrease in external energy dependence; a boost to local and regional component manufacturing industries; promotion of regional engineering and consultancy services specializing in the utilization of RE; increased R&D, decrease in impact of electricity production and transformation; increase in the level of services for the rural population; creation of employment, etc. [4].

Dincer [5] reported the linkages between energy and exergy, exergy and the environment, energy and sustainable development, and energy policy making and exergy in detail. He provided the following key points to highlight the importance of the exergy and its essential utilization in numerous ways: (a) it is a primary tool in best addressing the impact of energy resource utilization on the environment. (b) It is an effective method using the conservation of mass and conservation of energy principles together with the second law of thermodynamics for the design and analysis of energy systems. (c) It is a suitable technique for furthering the goal of more efficient energy–resource use, for it enables the locations, types, and true magnitudes of wastes and losses to be determined. (d) It is an efficient technique revealing whether or not and by how much it is possible to design more efficient energy systems by reducing the inefficiencies in existing systems. (e) It is a key component in obtaining a sustainable development.

Sustainable development does not make the world ‘ready’ for the future generations, but it establishes a basis on which the future world can be built. A sustainable energy system may be regarded as a cost-efficient, reliable, and environmentally friendly energy system that effectively utilizes local resources and networks. It is not ‘slow and inert’ like a conventional energy system, but it is flexible in terms of new techno-economic and political solutions. The introduction of new solutions is also actively promoted [6].

An exergy analysis (or second law analysis) has proven to be a powerful tool in the simulation thermodynamic analyses of energy systems. In other words, it has been widely used in the design, simulation and performance evaluation of energy systems. Exergy analysis method is employed to detect and to evaluate quantitatively the causes of the thermodynamic imperfection of the process under consideration. It can, therefore, indicate

the possibilities of thermodynamic improvement of the process under consideration, but only an economic analysis can decide the expediency of a possible improvement [7,8].

The concepts of exergy, available energy, and availability are essentially similar. The concepts of exergy destruction, exergy consumption, irreversibility, and lost work are also essentially similar. Exergy is also a measure of the maximum useful work that can be done by a system interacting with an environment which is at a constant pressure P_0 and a temperature T_0. The simplest case to consider is that of a reservoir with heat source of infinite capacity and invariable temperature T_0. It has been considered that maximum efficiency of heat withdrawal from a reservoir that can be converted into work is the Carnot efficiency [9,10].

Although numerous studies have been conducted on the energetic analysis and performance evaluation of RERs by using energy analysis method in the literature, very limited review papers have appeared on exergy analysis and performance assessment of RERs. In this regard, Koroneos et al. [11] dealt with the three kinds of RERs in terms of exergetic aspects, namely (i) exergetic analysis of a solar thermal power system by presenting a study conducted by Singh et al. [12], (ii) exergy analysis of geothermal power systems by presenting and evaluating the Larderello–Farinello–Valle Secolo Geothermal Area (Tuscany, Italy) studied by Bettagli and Bidini [13], and (iii) exergy analysis of wind energy systems by giving the relations used in the analysis and evaluating a wind energy system. They also made a comparison between renewable and non-RE sources, and concluded that some of the systems appear to had high efficiencies, and in some cases they are greater than the efficiency of systems using non-RE sources. In other cases, like the conversion of solar energy to electricity, the efficiencies were lower, in order to meet the electricity needs of cities. Hermann [14] identified the primary exergy reservoirs that supply exergy to the biosphere and quantified the intensive and extensive exergy of their derivative secondary reservoirs, or resources. Exergy relations of cosmic radiation exchange, wind, ocean surface waves, precipitation, ocean thermal gradient, tides and geothermal were also briefly presented.

The present study differs from the previous ones due to the facts that: (i) This covers a comprehensive exergetic analysis and performance evaluation of RERs. (ii) This includes a wide range of RERs such as solar, wind, geothermal and biomass along with their subsections (i.e., for geothermal, its direct and indirect applications) as well as hybrid systems. (iii) This presents a comparison between previously conducted studies in tabulated forms, and (iv) This summarizes exergetic utilization efficiency of RERs as done by Hepbasli and Utlu [15] for the first time for Turkey. In this regard, the structure of the paper is organized as follows: The first section includes the introduction; Section 2 deals with energy and exergy modeling, while general relations are described in Section 3; exergetic analysis and evaluating the RERs are treated in Section 4 in more detail by applying the general relations to various RERs; and the last section concludes.

2. Energy and exergy modeling

Dincer et al. [16] reported that, to provide an efficient and effective use of fuels, it is essential to consider the quality and quantity of the energy used to achieve a given objective. In this regard, the first law of thermodynamics deals with the quantity of energy and asserts that energy cannot be created or destroyed, whereas the second law of thermodynamics deals with the quality of energy, i.e., it is concerned with the quality of

energy to cause change, degradation of energy during a process, entropy generation and the lost opportunities to do work. More specifically, the first law of thermodynamics is concerned only with the magnitude of energy with no regard to its quality; on the other hand, the second law of thermodynamics asserts that energy has quality as well as quantity. By quality, it means the ability or work potential of a certain energy source having certain amount of energy to cause change, i.e., the amount of energy which can be extracted as useful work which is termed as exergy. First and second law efficiencies are often called energy and exergy efficiencies, respectively. It is expected that exergy efficiencies are usually lower than the energy efficiencies, because the irreversibilities of the process destroy some of the input exergy.

Exergy is the expression for loss of available energy due to the creation of entropy in irreversible systems or processes. The exergy loss in a system or component is determined by multiplying the absolute temperature of the surroundings by the entropy increase. Entropy is the ratio of the heat absorbed by a substance to the absolute temperature at which it was added. While energy is conserved, exergy is accumulated [17].

Exergy analysis provides a method to evaluate the maximum work extractable from a substance relative to a reference state (i.e., dead state). This reference state is arbitrary, but for terrestrial energy conversion the concept of exergy is most effective if it is chosen to reflect the environment on the surface of the Earth. The various forms of exergy are due to random thermal motion, kinetic energy, potential energy associated with a restoring force, or the concentration of species relative to a reference state. In order to establish how much work potential a resource contains, it is necessary to compare it against a state defined to have zero work potential. An equilibrium environment which cannot undergo an energy conversion process to produce work is the technically correct candidate for a reference state [14].

It should be noticed that exergy is always evaluated with respect to a reference environment (i.e. dead state). When a system is in equilibrium with the environment, the state of the system is called the dead state due to the fact that the exergy is zero. At the dead state, the conditions of mechanical, thermal, and chemical equilibrium between the system and the environment are satisfied: the pressure, temperature, and chemical potentials of the system equal those of the environment, respectively. In addition, the system has no motion or elevation relative to coordinates in the environment. Under these conditions, there is neither possibility of a spontaneous change within the system or the environment nor an interaction between them. The value of exergy is zero. Another type of equilibrium between the system and environment can be identified. This is a restricted form of equilibrium, where only the conditions of mechanical and thermal equilibrium (thermo-mechanical equilibrium) must be satisfied. Such state is called the restricted dead state. At the restricted dead state, the fixed quantity of matter under consideration is imagined to be sealed in an envelope impervious to mass flow, at zero velocity and elevation relative to coordinates in the environment, and at the temperature T_0 and pressure P_0 taken often as 25 °C and 1 atm [18].

3. General relations

For a general steady state, steady-flow process, the four balance equations (mass, energy, entropy and exergy) are applied to find the work and heat interactions, the rate of exergy decrease, the rate of irreversibility, the energy and exergy efficiencies [16,19–21].

3.1. Mass, energy, entropy and exergy balances

The mass balance equation can be expressed in the rate form as

$$\sum \dot{m}_{\text{in}} = \sum \dot{m}_{\text{out}}, \tag{1}$$

where $\dot{m}$ is the mass flow rate, and the subscript in stands for inlet and out for outlet.

The general energy balance can be expressed below as the total energy inputs equal to total energy outputs.

$$\sum \dot{E}_{\text{in}} = \sum \dot{E}_{\text{out}}. \tag{2}$$

In the absence of electricity, magnetism, surface tension and nuclear reaction, the total exergy of a system $\dot{\text{E}}\text{x}$ can be divided into four components, namely (i) physical exergy $\dot{\text{E}}\text{x}^{\text{PH}}$, (ii) kinetic exergy $\dot{\text{E}}\text{x}^{\text{KN}}$, (iii) potential exergy $\dot{\text{E}}\text{x}^{\text{PT}}$, and (iv) chemical exergy $\dot{\text{E}}\text{x}^{\text{CH}}$ [16].

$$\dot{\text{E}}\text{x} = \dot{\text{E}}\text{x}^{\text{PH}} + \dot{\text{E}}\text{x}^{\text{KN}} + \dot{\text{E}}\text{x}^{\text{PT}} + \dot{\text{E}}\text{x}^{\text{CH}}. \tag{3}$$

Although exergy is extensive property, it is often convenient to work with it on a unit of mass or molar basis. The total specific exergy on a mass basis may be written as follows:

$$\text{ex} = \text{ex}^{\text{PH}} + \text{ex}^{\text{KN}} + \text{ex}^{\text{PT}} + \text{ex}^{\text{CH}}. \tag{4}$$

The general exergy balance can be written as follows:

$$\sum \dot{\text{E}}\text{x}_{\text{in}} - \sum \dot{\text{E}}\text{x}_{\text{out}} = \sum \text{E}\dot{\text{x}}_{\text{dest}} \tag{5a}$$

or

$$\text{E}\dot{\text{x}}_{\text{heat}} - \text{E}\dot{\text{x}}_{\text{work}} + \text{E}\dot{\text{x}}_{\text{mass,in}} - \text{E}\dot{\text{x}}_{\text{mass,out}} = \text{E}\dot{\text{x}}_{\text{dest}} \tag{5b}$$

with

$$\text{E}\dot{\text{x}}_{\text{heat}} = \Sigma\left(1 - \frac{T_0}{T_k}\right)\dot{Q}_k, \tag{6a}$$

$$\text{E}\dot{\text{x}}_{\text{work}} = \dot{W}, \tag{6b}$$

$$\text{E}\dot{\text{x}}_{\text{mass,in}} = \Sigma\dot{m}_{\text{out}}\psi_{\text{out}}, \tag{6c}$$

$$\text{E}\dot{\text{x}}_{\text{mass,out}} = \Sigma\dot{m}_{\text{out}}\psi_{\text{out}}, \tag{6d}$$

where $\dot{Q}_k$ is the heat transfer rate through the boundary at temperature T_k at location k and $\dot{W}$ is the work rate.

The flow (specific) exergy is calculated as follows:

$$\psi = (h - h_0) - T_0(s - s_0), \tag{7}$$

where h is enthalpy, s is entropy, and the subscript zero indicates properties at the restricted dead state of P_0 and T_0.

The rate form of the entropy balance can be expressed as

$$\dot{S}_{\text{in}} - \dot{S}_{\text{out}} + \dot{S}_{\text{gen}} = 0, \tag{8}$$

where the rates of entropy transfer by heat transferred at a rate of $\dot{Q}_k$ and mass flowing at a rate of $\dot{m}$ are $\dot{S}_{\text{heat}} = \dot{Q}_k/T_k$ and $\dot{S}_{\text{mass}} = \dot{m}s$, respectively.

Taking the positive direction of heat transfer to be to the system, the rate form of the general entropy relation given in Eq. (8) can be rearranged to give

$$\dot{S}_{\text{gen}} = \Sigma \dot{m}_{\text{out}} s_{\text{out}} - \Sigma \dot{m}_{\text{in}} s_{\text{in}} - \Sigma \frac{\dot{Q}_k}{T_k}. \tag{9}$$

Also, it is usually more convenient to find $\dot{S}_{\text{gen}}$ first and then to evaluate the exergy destroyed or the irreversibility rate $\dot{I}$ directly from the following equation, which is called Gouy–Stodola relation [22]:

$$\dot{I} = \dot{\text{E}}\text{x}_{\text{dest}} = T_0 \dot{S}_{\text{gen}}. \tag{10}$$

The specific exergy (flow exergy) of an incompressible substance (i.e., water) is given by [22]

$$\psi_{\text{w}} = C\left(T - T_0 - T_0 \ln \frac{T}{T_0}\right). \tag{11}$$

The total flow exergy of air is calculated from [23]

$$\begin{aligned}\psi_{\text{a,t}} = {} & (C_{\text{p,a}} + \omega C_{\text{p,v}}) T_0 [(T/T_0) - 1 - \ln(T/T_0)] + (1 + 1.6078\omega) R_{\text{a}} T_0 \ln(P/P_0) \\ & + R_{\text{a}} T_0 \left\{ \frac{(1 + 1.6078\omega) \ln[(1 + 1.6078\omega_0)}{(1 + 1.6078\omega)] + 1.6078\omega \ln(\omega/\omega_0)} \right\},\end{aligned} \tag{12}$$

where the specific humidity ratio is

$$\omega = \dot{m}_{\text{v}}/\dot{m}_{\text{a}}. \tag{13}$$

Assuming air to be a perfect gas, the specific physical exergy of air is calculated by the following relation [24]

$$\psi_{\text{a,per}} = C_{\text{p,a}}\left(T - T_0 - T_0 \ln \frac{T}{T_0}\right) + R_{\text{a}} T_0 \ln \frac{P}{P_0}. \tag{14}$$

3.2. Energy and exergy efficiencies

Numerous ways of formulating exergetic (or exergy or second-law) efficiency (effectiveness, or rational efficiency) for various energy systems are given in detail elsewhere [20]. It is very useful to define efficiencies based on exergy (sometimes called *Second Law efficiencies*). Whereas there is no standard set of definitions in the literature, two different approaches are generally used—one is called l ‘‘brute-force’’, while the other is called ‘‘functional.’’ [25].

- A ‘‘brute-force’’ *exergy efficiency* for any system is defined as the ratio of the sum of all output exergy terms to the sum of all input exergy terms.
- A ‘‘functional’’ *exergy efficiency* for any system is defined as the ratio of the exergy associated with the desired energy output to the exergy associated with the energy expended to achieve the desired output.

Here, in a similar way, exergy efficiency is defined as the ratio of total exergy output to total exergy input, i.e.

$$\varepsilon = \frac{\dot{\mathrm{E}}\mathrm{x}_{\mathrm{output}}}{\dot{\mathrm{E}}\mathrm{x}_{\mathrm{input}}} = 1 - \frac{\dot{\mathrm{E}}\mathrm{x}_{\mathrm{dest}}}{\dot{\mathrm{E}}\mathrm{x}_{\mathrm{input}}}, \qquad (15)$$

where "output or out" stands for "net output" or "product" or "desired value" or "benefit", and "input or in" stands for "given" or "used" or "fuel".

It is clear that the brute-force definition can be applied in a straightforward manner, irrespective of the nature of the component, once all exergy flows have been determined. The functional definition, however, requires judgment and a clear understanding of the purpose of the system under consideration before the working equation for the efficiency can be formulated [25].

3.3. Exergetic improvement potential

Van Gool [26] has also proposed that maximum improvement in the exergy efficiency for a process or system is obviously achieved when the exergy loss or irreversibility ($\mathrm{E\dot{x}_{in}} - \mathrm{E\dot{x}_{out}}$) is minimized. Consequently, he suggested that it is useful to employ the concept of an exergetic "improvement potential" when analyzing different processes or sectors of the economy. This improvement potential in the rate form, denoted $\mathrm{I\dot{P}}$, is given by

$$\mathrm{I\dot{P}} = (1 - \varepsilon)(\mathrm{E\dot{x}_{in}} - \mathrm{E\dot{x}_{out}}). \qquad (16)$$

3.4. Some thermodynamic parameters

Thermodynamics analysis of RERs may also be performed using the following parameters [27]:

Fuel depletion ratio:

$$\delta_i = \frac{\dot{I}_i}{\dot{F}_\mathrm{T}}. \qquad (17)$$

Relative irreversibility:

$$\chi_i = \frac{\dot{I}_i}{\dot{I}_\mathrm{T}}. \qquad (18)$$

Productivity lack:

$$\xi_i = \frac{\dot{I}_i}{\dot{P}_\mathrm{T}}. \qquad (19)$$

Exergetic factor:

$$f_i = \frac{\dot{F}_i}{\dot{F}_\mathrm{T}}. \qquad (20)$$

4. Exergetic analysis and evaluation of renewable energy resources

4.1. Solar energy systems

In evaluating the performance of solar energy systems using exergy analysis method, calculation of the exergy of radiation is very crucial. However, its calculation is a problem of unquestionable interest, since exergy represents the maximum quantity of work that can be produced in some given environment (usually the terrestrial environment, considered as an infinite heat source or sink) [28]. Over a period of more than 20 years, many papers including various approaches to this calculation have been published, as reported in [29,30]. Among these, the first one [31], which is called by Petela [29,32] the maximum efficiency ratio (or exergy-to-energy ratio for radiation) for determining an exergy of thermal emission at temperature T, is as follows:

$$\psi_{\text{srad,max}} = 1 + \frac{1}{3}\left(\frac{T_0}{T}\right)^4 - \frac{4}{3}\frac{T_0}{T}, \tag{21}$$

where T was taken to equal the solar radiation temperature (T_s) with 6000 K in exergetic evaluation of a solar cylindrical-parabolic cooker and a solar parabolic-cooker by Petela [32] and Ozturk [33], respectively. Eq. (21) was also derived by Szargut [34] who presented a simple scheme of a reversible prime mover (different from that of Petela) transforming the energy of radiation into mechanical or electrical work and took into account that the solar radiation had a composition similar to that of a black body.

The history of Eq. (21) is as follows [35]: It was first derived by Petela [31] and independently by Landsberg and Mallinson [36] and Press [37], while Spanner [38] proposed Petela's equation for the direct solar radiation exergy [29]. As a consequence, it is sometimes called the Landsberg efficiency [34], the Petela–Landsberg upper bound [39], or, more appropriately, the Petela–Press–Landsberg and Mallinson formula [28].

Petela [29] reported that in the existing literature in the above field, the most discussed formulae for heat radiation exergy were those derived by him [31], Spanner [38] and Jeter [40] given in Eqs. (21), (24b), and (24c), respectively. As for as the application of these equations to various thermal systems by some investigators, Chaturvedi et al. [41] used Eq. (21) in the performance assessment of a variable capacity direct expansion solar-assisted heat pump system for domestic hot water application. Eskin [42] considered Eq. (24b) in evaluating the performance of a solar process heating system, while Singh et al. [12], and Ucar and Inalli [43] considered Eq. (24c) in the exergetic analysis of a solar thermal power plant and the exergoeconomic analysis of a solar-assisted heating system, respectively.

Petela [29] also listed three various limiting energy efficiencies of utilization of the radiation matter in Table 1 [29] and explained them as follows: ''Bejan's conclusion was that all theories (Spanner's, Jeter's and Petela's) concerning the ideal conversion of thermal radiation into work, although obtaining different results, were correct. Although really correct, they had incomparable significance for the true estimation of the radiation exergy value. All of the efficiencies assumed work as an output. However, Petela's work was equal to the radiation exergy, Jeter's work was the heat engine cycle work and Spanner's work was an absolute work. As an input, Petela and Spanner assumed the radiation energy, whereas Jeter assumed heat [29].''

Table 1
Numerators (output) and denominators (input) of the limiting energy efficiency of radiation utilization by three different researchers [29]

Investigators	Input	Output	Unified efficiency expression	
Petela [31]	Radiation energy	Useful work = radiation exergy	$1+\frac{1}{3}\left(\frac{T_0}{T}\right)^4-\frac{4}{3}\frac{T_0}{T}$	(21′)
Spanner [38]	Radiation energy	Absolute work	$1-\frac{4}{3}\frac{T_0}{T}$	(24b)
Jeter [40]	Heat	Net work of a heat engine	$1-\frac{T_0}{T}$	(24c)

Svirezhev et al. [44] applied a new concept regarding the exergy of solar radiation to the analysis of satellite data describing the seasonal (monthly) dynamics of four components of the global radiation balance: incoming and outgoing short and long-wave solar radiation. They constructed maps of annual mean exergy and some derivative values using real satellite data. They concluded that exergy could be a good indicator for crucial regions of the oceans, which were indicated where its values were maximal.

4.1.1. Solar collector applications

The instantaneous exergy efficiency of the solar collector can be defined as the ratio of the increased water exergy to the exergy of the solar radiation [33]. In other words, it is a ratio of the useful exergy delivered to the exergy absorbed by the solar collector [12].

$$\varepsilon_{\rm scol}=\frac{\dot{\rm E}{\rm x}_{\rm u}}{\dot{\rm E}{\rm x}_{\rm scol}} \tag{22}$$

with

$$\dot{\rm Ex}_{\rm u}=\dot{m}_{\rm w}[(h_{\rm w,out}-h_{\rm w,in})-T_0(s_{\rm w,out}-s_{\rm w,in})] \tag{23a}$$

or

$$\dot{\rm Ex}_{\rm u}=\dot{m}_{\rm w}C_{\rm w}\left[(T_{\rm w,out}-T_{\rm w,in})-T_0\left({\rm Ln}\frac{T_{\rm w,out}}{T_{\rm w,in}}\right)\right], \tag{23b}$$

$$\dot{\rm Ex}_{\rm u}=\dot{Q}_{\rm u}\left[1-\frac{T}{T_{\rm w,out}-T_{\rm w,in}}\left({\rm Ln}\frac{T_{\rm w,out}}{T_{\rm w,in}}\right)\right] \tag{23c}$$

and

$$\dot{\rm Ex}_{\rm scol}=AI_{\rm T}\psi_{\rm srad,max}, \tag{24a}$$

where the subscripts "in" and "out" denote the inlet and outlet of the solar collector, respectively, while $\psi_{\rm srad,max}$ may also be calculated using Eqs. (21), (24b) and (24c) given in Table 1 [29].

The exergy of solar radiation with beam ($I_{\rm be}$) and diffuse ($I_{\rm d}$) components for parabolic collectors is also given by the following equation [45], which was used by Eskin [46] in the performance evaluation of a cylindrical parabolic concentrating collector.

$$\psi_{\rm srad,be,d}=I_{\rm be}\left(1-\frac{4T_0}{3T_{\rm s}}\right)+I_{\rm d}\left(1-\frac{4T_0}{3T_{\rm s}^*}\right) \tag{25}$$

with

$$\frac{T_s}{T_s^*} = 0.9562 + 0.2777\,\ln(1/\kappa) + 0.0511\kappa, \tag{26}$$

where κ is the dilution factor of diffuse radiation [47].

4.1.1.1. Solar water heating systems. Solar water heater is the most popular means of solar energy utilization because of technological feasibility and economic attraction compared with other kinds of solar energy utilization. Fig. 1 illustrates a schematic of a typical domestic-scale solar water heater, which mainly consists of a solar collector and a storage barrel [48].

Exergy efficiency of the domestic-scale solar water heater may be calculated using Eq. (15) as follows:

$$\varepsilon_{s,\mathrm{heater}} = \frac{\dot{\mathrm{E}}\mathrm{x}_{\mathrm{output}}}{\dot{\mathrm{E}}\mathrm{x}_{\mathrm{sun}}}, \tag{27}$$

where exergy from the storage barrel to the end-user (output exergy) may be written as follows [48], assuming the temperature distribution in the storage barrel is linear:

$$\begin{aligned} \mathrm{E}\dot{\mathrm{x}}_{\mathrm{output}} = {} & \dot{m}_{\mathrm{w}} C_{\mathrm{w}}\left(\frac{T_{\mathrm{top}} + T_{\mathrm{bottom}}}{2} - T_0\right) - \dot{m}_{\mathrm{w}} C_{\mathrm{w}} T_0\left(\ln\frac{T_{\mathrm{top}}}{T_0} - 1\right) \\ & - \frac{T_{\mathrm{bottom}} T_0 \dot{m}_{\mathrm{w}} C_{\mathrm{w}}}{T_{\mathrm{top}} - T_{\mathrm{bottom}}} \ln\frac{T_{\mathrm{top}}}{T_{\mathrm{bottom}}} \end{aligned} \tag{28}$$

and $\mathrm{E}\dot{\mathrm{x}}_{\mathrm{sun}}$ is the exergy from sun (input exergy) and may be found using Eq. (24a).

The collector exergy efficiency is calculated by the following equation, while it may be found using Eqs. (22), (23b) and (24).

$$\varepsilon_{s,\mathrm{col}} = \frac{\dot{\mathrm{E}}\mathrm{x}_{\mathrm{col,tank}}}{\dot{\mathrm{E}}\mathrm{x}_{\mathrm{sun}}}, \tag{29}$$

where $\mathrm{E}\dot{\mathrm{x}}_{\mathrm{col,tank}}$ is exergy from the collector to the storage barrel and may be written in a similar way given by Eq. (23b) as follows [48].

$$\mathrm{E}\dot{\mathrm{x}}_{\mathrm{col,tank}} = \dot{m}_{\mathrm{w}} C_{\mathrm{w}}\left[(T_{\mathrm{w,out}} - T_0) - T_0\left(\ln\frac{T_{\mathrm{w,out}}}{T_0}\right)\right]. \tag{30}$$

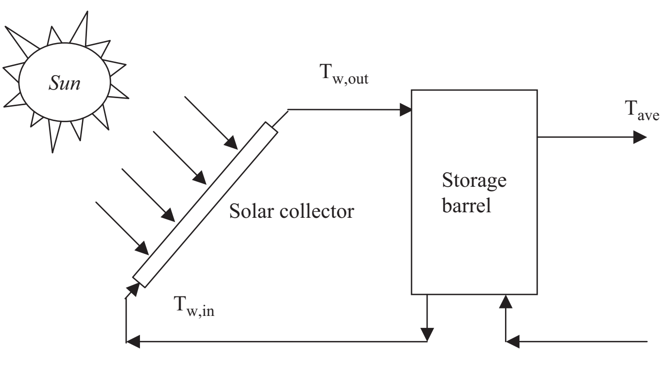


Fig. 1. A typical domestic-scale solar water heater [48].

Xiaowu and Ben [48] performed an exergy analysis of a domestic-scale solar heater. They used the data obtained from Domestic-Scale Solar Water Heaters Performance Testing Station, located in Yun Nan province, China as follows: Top and bottom hot water temperatures of 50 and 38 °C in the storage barrel, respectively, 2.5 m^2 of collector area, an average ambient temperature of 25 °C, an average ambient water temperature of 24 °C, 466 W/m^2 of whole-day average solar radiation and 196.4 kg of water storing log capacity for the storage barrel. They calculated the exergy efficiency value of the solar water heater using the above data and found to be 0.77%. The main conclusions drawn from the results of their study were as follows: The exergy efficiency of domestic-scale water heater was small as the output energy was of low quality. The storage barrel had large exergy losses. It was worthwhile to design a new style of storage barrel for reducing unnecessary mixing of water. In order to improve the exergy efficiency of domestic-scale water heater, a judicious choice of width of plate and layer number of cover was necessary [48].

4.1.1.2. Solar space heating and cooling

4.1.1.2.1. Air systems. Air systems are indirect water heating systems that circulate air via ductwork through the collectors to an air-to-liquid heat exchanger. In the heat exchanger, heat is transferred to the potable water, which is also circulated through the heat exchanger and returned to the storage tank. A double storage tank system is shown in Fig. 2 [48]. This type of system is used most often, because air systems are generally used for preheating domestic hot water and thus auxiliary is used only in one tank. The main advantage of the system is that air does not need to be protected from freezing or boiling, is noncorrosive, and is free. The disadvantages are that air handling equipment (ducts and fans) need more space than piping and pumps, air leaks are difficult to detect, and parasitic power consumption is generally higher than that of liquid systems [49].

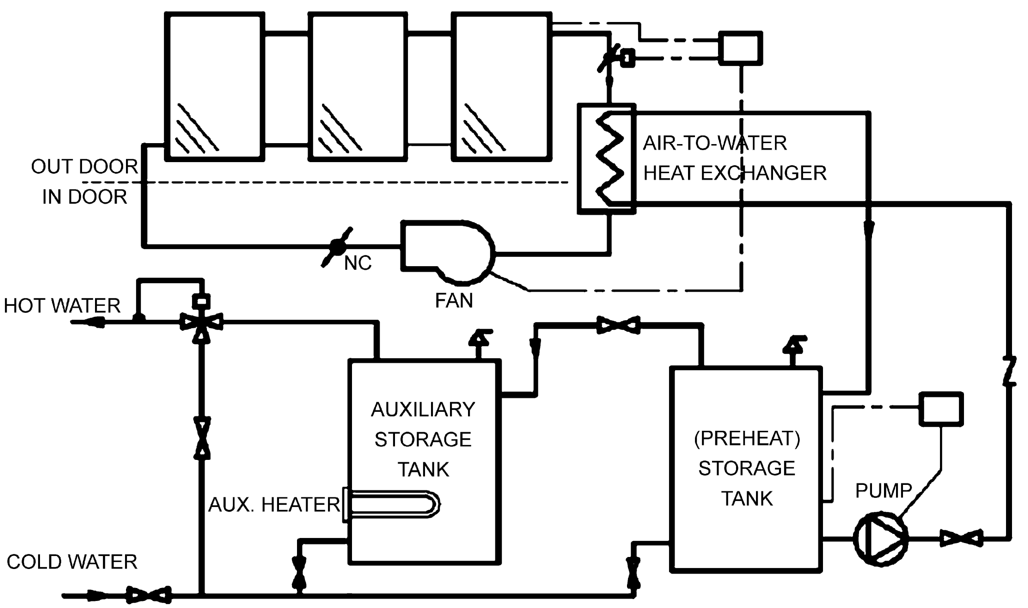


Fig. 2. A schematic of air system with a double storage tank drawn by Xiaowu and Ben [48].

The relations used to evaluate air systems using exergy analysis method are presented by the author since any exergetic assessment based on the actual data could not be found. The main parts to be included in the exergy analysis are (I) air solar collector, (II) air-to-water hat exchanger, (III) fan, (IV) storage tank and (V) circulating pump. The exergy destruction and exergy efficiency relations for each component of the whole air system are given below using Eqs. (5a) and (15), respectively.

I. *Air solar collector*:

$$\dot{E}x_{dest,I} = \dot{E}x_{in,air} - \dot{E}x_{out,air} + \dot{E}x_{s}, \tag{31}$$

$$\varepsilon_{I} = \frac{\dot{E}x_{out,air} - \dot{E}x_{in,air}}{\dot{E}x_{scol}}, \tag{32}$$

where $\dot{E}x_{in,air}$ and $\dot{E}x_{out,air}$ are calculated using Eqs. (6c), (6d), (12) and (14), while $\dot{E}x_{scol}$ is found from Eq. (24a).

II. *Air-to-heat exchanger*:

$$\dot{E}x_{dest,II} = (\dot{E}x_{hot,air,in} + \dot{E}x_{cold,w,in}) - (\dot{E}x_{hot,air,out} + \dot{E}x_{cold,w,out}), \tag{33}$$

$$\varepsilon_{II} = \frac{\dot{E}x_{cold,w,out} - \dot{E}x_{cold,w,in}}{\dot{E}x_{hot,air,in} - \dot{E}x_{hot,air,out}} = \frac{\dot{m}_{cold,w}(\psi_{cold,w,out} - \psi_{cold,w,in})}{\dot{m}_{hot,air}(\psi_{hot,air,in} - \psi_{hot,air,out})}. \tag{34}$$

III. *Fan*:

$$\dot{E}x_{dest,III} = \dot{W}_{fan,e} + \dot{m}_{air}(\psi_{out,air} - \psi_{in,air}), \tag{35}$$

$$\varepsilon_{III} = \frac{\dot{E}x_{out} - \dot{E}x_{in}}{\dot{W}_{fan}} = \frac{\dot{m}_{air}(\psi_{out,air} - \psi_{in,air})}{\dot{W}_{fan}} \tag{36}$$

with

$$\dot{W}_{fan} = \dot{m}_{air}\left[(h_{out,air} - h_{in,air}) + \frac{V_{exit}^2}{2}\right]. \tag{37}$$

IV. *Storage tank*:

$\dot{E}x_{dest,IV}$ and ε_{IV} may be calculated in a similar way given by Eqs. (33) and (34).

V. *Circulating pump*:

$$\dot{E}x_{dest,VI} = \dot{m}_{w}(\psi_{in} - \psi_{out,a}) + \dot{W}_{pump,e}, \tag{38}$$

$$\varepsilon_{V} = \frac{\dot{E}x_{out,a} - \dot{E}x_{in}}{\dot{W}_{pump,e}} = \frac{\dot{m}_{w}(\psi_{out,a} - \psi_{in})}{\dot{W}_{pump,e}} \tag{39}$$

with

$$\dot{W}_{pump,e} = \dot{W}_{pump}/(\eta_{pump,e}\eta_{pump,mech}), \tag{40}$$

where $\eta_{pump,e}$ and $\eta_{pump,mech}$ are the circulating pump motor electrical and circulating pump mechanical efficiencies.

The overall exergy destruction in the whole air system is calculated as follows, while the overall exergy efficiency is found on a product/fuel basis given by Eq. (15).

$$\dot{Ex}_{dest,o} = \dot{Ex}_{dest,I} + \dot{Ex}_{dest,II} + \dot{Ex}_{dest,III} + \dot{Ex}_{dest,IV} + \dot{Ex}_{dest,V}. \tag{41}$$

4.1.1.2.2. Water systems. There are many variations of systems used for solar space heating. The exergetic analysis of these systems may be performed using relations given in Sections 4.1.1.1 and 4.1.1.2.1.

4.1.1.2.3. Heat pumps. Heat pumps are preferred and widely used in many applications due to their high utilization efficiencies compared to conventional heating and cooling systems. There are two common types of heat pumps: air-source heat pumps and ground-source (geothermal) heat pumps (GSHPs). The main components of these systems are a compressor, a condenser, an expansion valve and an evaporator. In addition, circulating pumps and fans are used. GSHPs are exergetically studied in more detail in Section 4.3.2.2 and relevant exergy relations are presented in a tabulated form, while studies conducted by various investigators are compared. The relations given in these sections may be used in modeling and exergetic evaluation for heat pump systems. In case that a solar assisted heat pump with direct expansion of the refrigerant within the solar collector is used, the collector–evaporator part may be analyzed using Eq. (24a) for solar radiation input.

Tsaros et al. [50] studied on exergy analysis of heat pumps. Exergy transports between the components, to the loads and to the environment were assessed. The exergy consumption in each component were also determined. Typical results were presented for the operation of a nominal 3.5 ton residential air-to-air heat pump, in both the heating and cooling modes. Exergy efficiency values for various system components are listed in Table 2 [50]. Of the major components, the outdoor coil had the highest exergy efficiency, followed by the compressor and the indoor coil. The exergy efficiency of the indoor coil varied greatly with load and exceeded that of the compressor under some conditions. The fans, with the values less than 5%, were the least efficient [50].

Bilgen and Takahashi [51] carried out exergy analysis of heat pump—air conditioner systems. The experimental system, shown in Fig. 3 [51], was Matsushita room air conditioner CS-XG28M. The irreversibilities due to heat transfer and friction were considered. The coefficient of performance based on the first law of thermodynamics as a function of various parameters, their optimum values, and the efficiency and coefficient of performance based on exergy analysis were derived. Based on the exergy analysis, a simulation program was developed to simulate and evaluate experimental systems. It was found that the exergy efficiency varied from 37% to 25% both a decreasing function of heating or cooling load. The exergy destructions in various components were also determined for further study and improvement of its performance. It was suggested that to improve the performance of the heat pump system, each component could be further studied from exergy usage and economics points of view. Eventually, a system exergy-economics optimization study could be carried out to identify each component's relative importance with respect to operational conditions.

Table 2
Exergy efficiency values of the system components [50]

Component	Exergy efficiencies in % at various outdoor temperatures		
	−18.75 °C (17°F)	8.33 °C (47°F)	35 °C (95°F)
Indoor coil	82.6	57.0	35.3
Compressor, 4-way valve, outdoor coil, throttle	36.0	40.8	29.8
Compressor, 4-way valve, outdoor coil	44.0	47.7	35.2
Throttle	81.6	85.5	84.5
Compressor, 4-way valve	47.9	55.0	53.7
Outdoor coil	92.0	86.9	65.6
Compressor	50.5	58.5	58.3
4-way valve	94.7	93.9	92.1
Outdoor fan and motor	4.41	4.41	4.41
Indoor fan and motor	3.49	3.49	5.81
Overall without fans	30.1	23.4	10.7
Overall	21.7	18.1	8.43

Compressor includes associated hardware, while 4-way valve includes piping to coils.

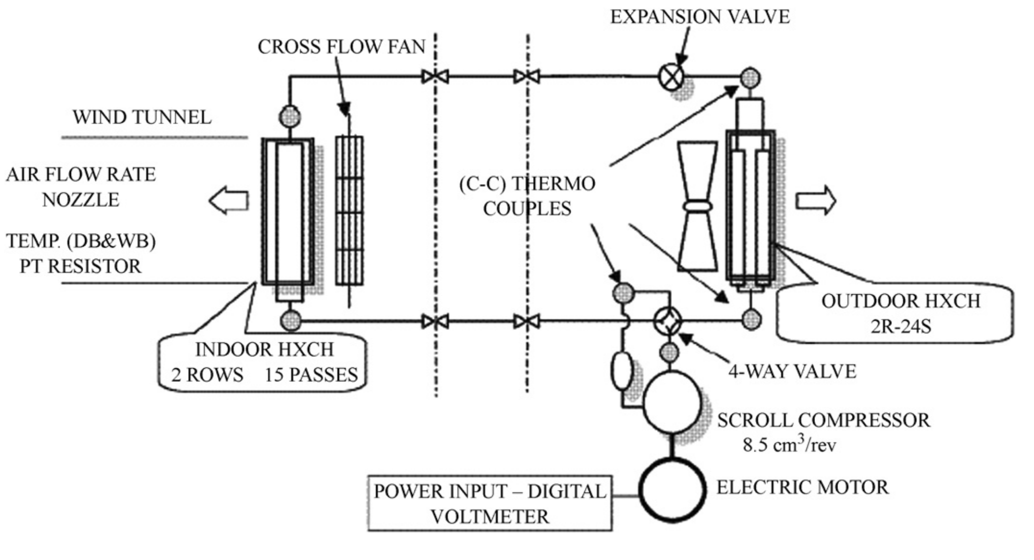


Fig. 3. Schematic of the experimental set up showing measurement system and instrumentation drawn by Bilgen and Takahashi [51].

Aprea et al. [52] studied on the performances of a vapor compression experimental system working both as a water chiller and as a heat pump, using as refrigerant fluids R22 and its substitute R417A (R125/R134a/R600 46.6/50/3.4% in mass). This kind of system has been used in industrial processing or air conditioning plants where a supply of refrigerated and heated water was required. The experimental system was principally made up of a unit that could operate both as refrigeration system and heat pump. It was made up of a hermetic compressor Scroll, a plate-type water heat exchanger inserted in a water tank, a finned tube air heat exchanger, two thermostatic expansion valves.

Aprea et al. [52] evaluated the efficiency defect for each component of the system, considering the ratio between the exergy destroyed in each one and the exergy required to sustain the process (i.e., the electrical power supplied to the compressor). The efficiency defects of R417A were always higher than the defects of R22 of about 6% related to the valve and the heat exchangers, and of about 10% referring to the compressor. Moreover, it was experimentally verified that the COP of R22 was higher than that of R417A also of about 18% related to the water chiller system and of about 15% referring to the heat pump.

Ma and Li [53] exergetically analyzed a heat pump system with economizer coupled with scroll compressor illustrated in Fig. 4 [53] and derived expressions for exergy losses of the processes in the system, exergy loss ratio and efficiency of the system. They also determined the exergetical losses and efficiency of this heat pump system using experimental data, while they assessed characteristics of exergy variation and transport and exergetic efficiency of the system. The experimental system studied is explained in more detail elsewhere [54].

Using Eq. (15), Ma and Li [53] expressed exergy efficiency as a ratio of the effective exergy output of the heat pump (equal to the heat load exergy in the condenser plus the cool capacity exergy in the evaporator) to the exergy of the electrical energy as follows:

$$\varepsilon = \frac{\dot{E}x_{\mathrm{eff,output}}}{\dot{E}x_{\mathrm{input}}} = \frac{E\dot{x}_{\mathrm{h}} + E\dot{x}_{\mathrm{cool}}}{E\dot{x}_{\mathrm{e}}} \tag{42}$$

From the distribution of the exergy loss, it was found that the maximum loss occurred in the compressor, accounting for about 82% of the total exergy destruction. This value would increase when the temperature difference between the condensation and the evaporation could be increased. The compressor was a bottleneck for the efficiency of the heat pump system, and increasing energy efficiency ratio for the compressor was crucial to the improvement of the heat pump system. For hermetic compressor, there were two mechanisms for exergy to consumption: one is was the process in which electrical power was converted to mechanical work in motor, and the other was the process of the mechanical work being converted to the pressure energy of the refrigerant in the compressor. The exergy losses in the evaporator and condenser were found to be 8.9% and

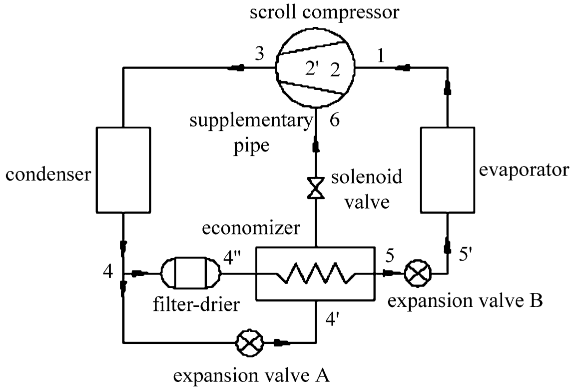


Fig. 4. Schematic of a heat pump system with economizer coupled with scroll compressor drawn by Ma and Li [53].

5.3% of the total loss, respectively, and were 10.8% and 6.5% of the loss in the compressor. Although they were relatively small compared with the loss in the compressor, minimizing the exergy losses in evaporator and condenser was also important for the improvement of the efficiency of the heat pump, and improving the evaporator was more beneficial for the overall system efficiency than improving the condenser. The exergy losses existing in the essential components of the heat pump system such as the compressor, the evaporator and the condenser were predominant in the total exergy loss, namely 96.2% of the total. In summary, the best gain in the heat pump system performance could be obtained through improvement in the compressor, followed by the evaporator and condenser. Using Eq. (42), exergy efficiency of the air-source heat pump system was determined to vary approximately from 33% to 42% at the evaporation temperatures of −25 to −12 °C with a fixed condensing temperature of 45 °C [53].

Badescu [55] proposed a model for the heating system of an ecological building whose main energy source was solar radiation. The most important component of the heating system was a vapor compression heat pump. The building's electric energy was provided by a photovoltaic (PV) array or from the AC grid, when necessary. Exergy analysis of the heat pump was performed. The state parameters and the process quantities were evaluated by using, as input, the building thermal load. It was reported that most of the exergy losses occurred during compression and condensation. Preliminary results indicated that the PV array could provide all the energy required to drive the heat pump compressor, if an appropriate electrical energy storage system was provided. In the analysis, meteorological data measured by the Romanian Meteorological and Hydrological Institute during 1961 in Bucharest (latitude 44.5°N, longitude 26.2°E, altitude 131 m above sea level) were used, while the exergy efficiency of the heat pump, was found using the following equation:

$$\varepsilon_{HP} = \frac{w_{comp,C}}{w_{comp,a}}, \tag{43}$$

where $w_{comp,a}$ and $w_{comp,C}$ are the specific mechanical works entering the actual and reversible (Carnot) compressor, respectively. Using Eq. (43), exergy efficiency of the heat pump was found to be 15.53% and 18.37% for the refrigerants of R114 and R12, respectively, based on the results obtained in the cold day of January 22, 1961 at 6.00 a.m. in Bucharest, when the ambient temperature was 255.7 K [55].

Cervantes and Torres-Reyes [56] performed an experimental study of a solar assisted heat pump with direct expansion of the refrigerant within the solar collector and evaluated the performance of this system using exergy analysis method. The condensation of the refrigerant took place in an R22/air condenser made out of stainless-steel, with a heat transfer area of 9.8 m^2. The compression stage was carried out by a hermetic compressor, and the expansion of R-22 occurred in a thermal expansion valve. The refrigerant was evaporated inside an uncovered solar flat collector, with a collection area of 364.5 m^2. Experimental tests were performed at a solar radiation range of 200–1100 W/m^2 and ambient temperatures varying from 20 to 32 °C. The actual amount of work supplied to the compressor, given by the electricity consumption, ranged from 1.1 to 1.36 kW. The maximum exergy efficiency, defined as the ratio of the outlet to the inlet exergy flow in every component of the heat pump cycle, was determined taking into account the typical parameters and performance coefficients. The results of this exergy analysis pointed out that the main source of irreversibility could be found in the evaporator of

the heat pump (i.e.,the solar collector) emphasizing that incoming solar radiation, as shown in Fig. 5 [56]. A full analysis of the inlet and outlet exergy flows and the main parameters associated to them, for each component of the solar assisted heat pump, is given in Ref. [57].

Ucar and Inalli [43] developed an exergoeconomic model for analysis and optimization of solar-heating systems with residential buildings. The model system consisted of flat plate solar collectors, a heat pump, an underground storage tank and a heating load, as shown in Fig. 6 [43]. The heat produced by the solar collectors was stored in underground storage tanks throughout the year. This heat was only extracted during the heating season. It was found from the exergetic analysis results for the cylindrical tank system that the largest exergy losses occurred in the house at 78.7%, followed by the heat pump at 40.9%, the collector at 39.7% and the storage at 19.8%.

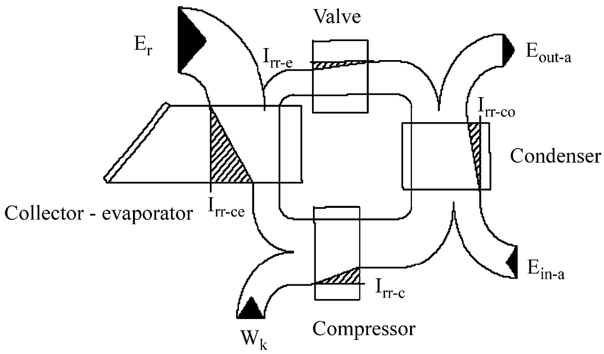


Fig. 5. Grassmann (exergy flow) diagram of the solar assisted heat pump system with direct expansion of the refrigerant within the solar collector drawn by Cervantes et al. [56].

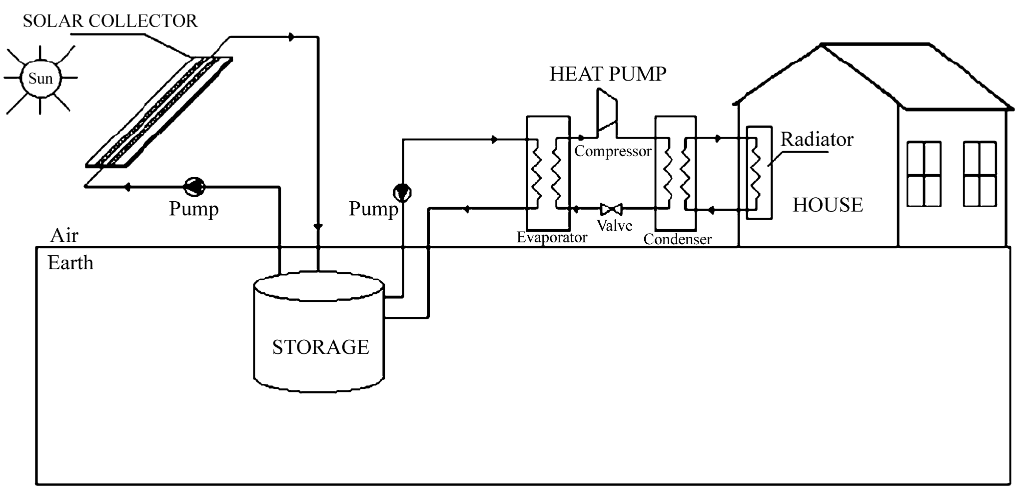


Fig. 6. Schematic diagram of a solar-assisted heating system for residential buildings drawn by Ucar and Inalli [43].

4.1.1.3. Solar refrigeration

4.1.1.3.1. Solar-driven ejector refrigeration systems. A solar-driven ejector refrigeration system consists of a solar collector subsystem and an ejector refrigeration subsystem. The major components in the refrigeration cycle are an ejector, a condenser, a generator, an evaporator, an expansion device and a pump. Fig. 7 [58] illustrates a schematic of this system, which was energetically analyzed by Pridasawas and Lundqvist [58] in more detail. In assessing this system using exergy analysis method, the relations given in Section 4.3.2.2 and additionally the exergetic efficiency definitions explained below may be used.

The exergy inputs and outputs may take different forms, e.g., radiation, heat or electricity. Thus, the exergetic efficiency of the ejector refrigeration cycle is defined as the ratio of the cooling exergy (at the evaporator) and the exergy inputs to the generator and the pump:

$$\varepsilon_{ej} = \frac{\text{E}\dot{\text{x}}_{evap}}{\text{E}\dot{\text{x}}_{g} + \text{E}\dot{\text{x}}_{p,e}} \tag{44}$$

with

$$\text{E}\dot{\text{x}}_{g} = \dot{Q}_{g}\left(1 - \frac{T_0}{T_g}\right), \tag{45}$$

where $\dot{Q}_g$ is energy input to the generator and T_g is the generating temperature [58].

The system exergetic efficiency is defined as the ratio of the cooling exergy and the exergy of the available solar heat input plus the electricity input to the pump:

$$\varepsilon_{sys} = \frac{\text{E}\dot{\text{x}}_{evap}}{\text{E}\dot{\text{x}}_{s,h} + \text{E}\dot{\text{x}}_{p,e}} \tag{46}$$

with

$$\text{E}\dot{\text{x}}_{s,h} = \dot{Q}_{ava}\left(1 - \frac{T_0}{T_{scol}}\right), \tag{47}$$

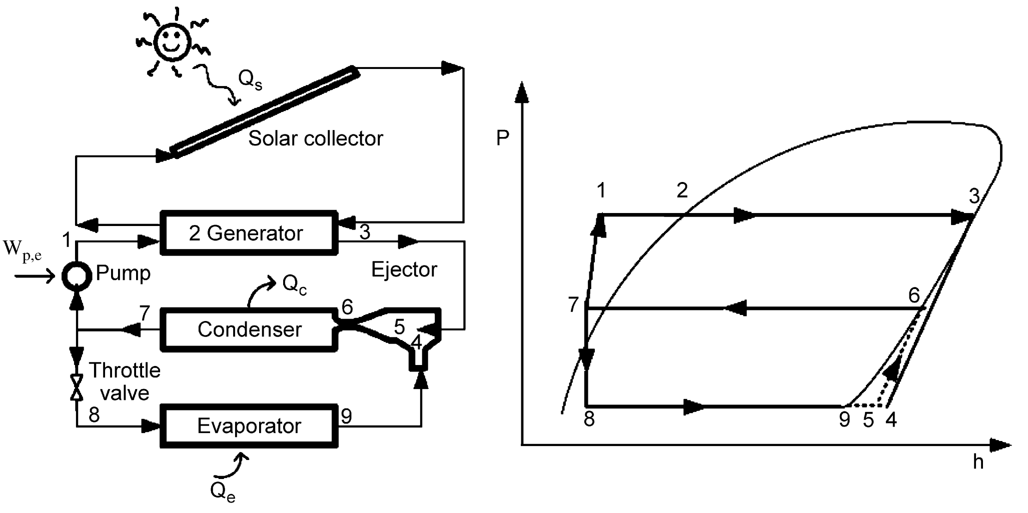


Fig. 7. Ejector refrigeration cycle drawn by Pridasawas and Lundqvist [58].

where $\dot{Q}_{ava}$ is available heat for the process in the solar collector and T_{scol} is the average temperature of the solar collector [58].

Pridasawas and Lundqvist [58] used the following relation established by De Vos [59] for calculating the exergy input to the collector per unit area as a function of the exergy emitted from the sun minus the albedo of the earth and the radiation emitted from the solar collector:

$$\dot{Ex}_{scol} = f\sigma T_s^4 + (1-f)\sigma T_{planet}^4 - \sigma T_{scol}^4, \tag{48}$$

where f is the sunlight dilution factor, which equal to 2.16×10^{-5} on the earth, σ is Stefan–Boltzmann constant ($5.67 \times 10^{-8}\,W/m^2\,K^4$), T_s is the temperature of the sun (K) and T_{planet} is the temperature of the planet (K).

The exergy loss during the transformation from solar radiation to heat on the solar collector is given as [58]:

$$\dot{I}_{scol,trans} = \dot{Ex}_s - \dot{Ex}_{s,h}. \tag{49}$$

The exergy loss from the exergy input to the solar collector to the working fluid can be calculated using the following equations [58]:

$$\dot{I}_{scol} = \dot{Ex}_{s,h} - \dot{Ex}_u \tag{50}$$

with

$$\dot{Ex}_u = \dot{Q}_u\left(1 - \frac{T_s}{T_{scol}}\right). \tag{51}$$

Pridasawas and Lundqvist [58] evaluated the performance of an ejector refrigeration cycle driven by solar energy using exergy analysis method. The analysis was based on the following conditions: a solar radiation of $700\,W/m^2$, an evaporator temperature of $10\,°C$, a cooling capacity of 5 kW, butane as the refrigerant in the refrigeration cycle and ambient temperature of $30\,°C$ as the reference temperature. Irreversibilities occurred among components and depend on the operating temperatures. The most significant losses in the system were in the solar collector and the ejector. The latter decreased inversely proportional to the evaporation temperature and dominated the total losses within the system. For the above operating conditions, the optimum generating temperature was about $80\,°C$. The exergy losses in the ejector refrigeration cycle is shown in Fig. 8 [58]. The highest loss with about 50.5% was found in the solar collector, followed by the losses in the ejector, which was 15.8% and in the condenser with 10.6% (1.49 kW = 0.89 kW loss and 0.60 kW rejected). On the component basis of the ejector refrigeration subsystem, the largest loss (32%) occurred in the ejector followed by the generator (22%), the condenser (21%). The rest of the exergy loss occurred in the pump, the evaporator and the expansion valve. The exergetic efficiency values for the solar collector and refrigeration cycle were 14.53 and 4.39%, respectively, while the overall exergetic efficiency was 0.66%.

4.1.1.3.2. Absorption units. Sozen et al. [60] investigated a prototype of an aqua–ammonia absorption heat pump system using solar energy. Fig. 9 [60] illustrates a schmatic of this system. The aqua–ammonia absorption heat pump consisted of condenser, evaporator, absorber, generator, pump, expansion valves, refrigerant heat exchanger (precooler, RHE) and mixture heat exchanger (solution heat exchanger, MHE). When these two heat exchangers were used in the system, the performance was increased.

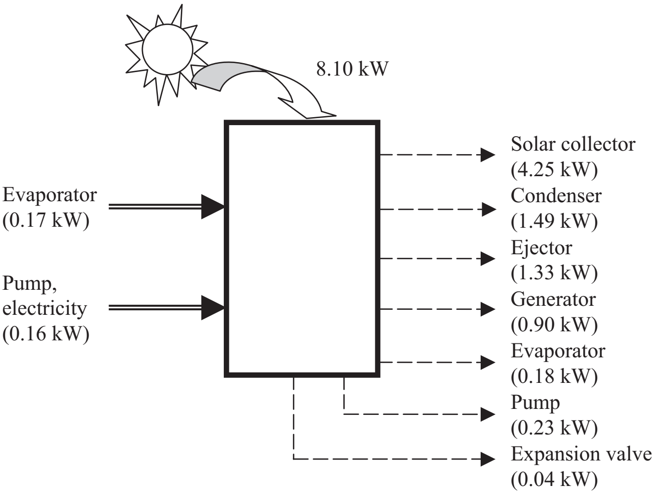


Fig. 8. Exergy balance of a solar-driven ejector refrigeration system for the generating temperature of 90°C and evaporation temperature of 10 °C [58].

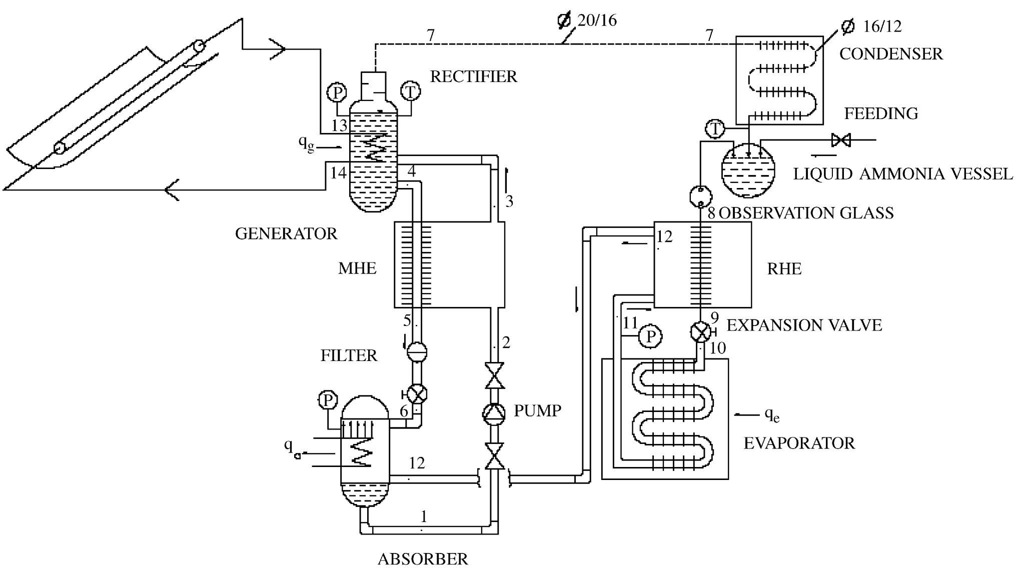


Fig. 9. Schematic of a absorption heat pump drawn by Sozen et al. [60].

For each individual component of the system shown in Fig. 9, the exergy destructions are written as follows [60]:

$$\dot{\mathrm{E}}\mathrm{x}_{\mathrm{dest,cond}} = \dot{m}_7(\dot{\mathrm{E}}\mathrm{x}_7 - \dot{\mathrm{E}}\mathrm{x}_8) - \dot{Q}_{\mathrm{cond}}[1 - (T_0/T_{\mathrm{cond}})], \tag{52}$$

$$\dot{\mathrm{E}}\mathrm{x}_{\mathrm{dest,evap}} = \dot{m}_7(\dot{\mathrm{E}}\mathrm{x}_{10} - \dot{\mathrm{E}}\mathrm{x}_{11}) + \dot{Q}_{\mathrm{evap}}[1 - (T_0/T_{\mathrm{evap}})], \tag{53}$$

$$\dot{\mathrm{E}}\mathrm{x}_{\mathrm{dest,absor}} = \dot{m}_7\dot{\mathrm{E}}\mathrm{x}_{12} + \dot{m}_6\dot{\mathrm{E}}\mathrm{x}_6 - \dot{m}_1\dot{\mathrm{E}}\mathrm{x}_1 - \dot{Q}_{\mathrm{absor}}[1 - (T_0/T_{\mathrm{absor}})], \tag{54}$$

$$\dot{\mathrm{E}}\mathrm{x}_{\mathrm{dest,pump}} = \dot{m}_1(\dot{\mathrm{E}}\mathrm{x}_1 - \dot{\mathrm{E}}\mathrm{x}_2) + \dot{W}_{\mathrm{pump,e}}, \tag{55}$$

$$\dot{\mathrm{E}}\mathrm{x}_{\mathrm{dest,g}} = \dot{m}_3\dot{\mathrm{E}}\mathrm{x}_3 - \dot{m}_4\dot{\mathrm{E}}\mathrm{x}_4 - \dot{m}_7\dot{\mathrm{E}}\mathrm{x}_7 + \dot{Q}_{\mathrm{g}}[1 - (T_0/T_{\mathrm{g}})], \tag{56}$$

$$\dot{\mathrm{E}}\mathrm{x}_{\mathrm{dest,mix,HE}} = \dot{m}_2(\dot{\mathrm{E}}\mathrm{x}_2 - \dot{\mathrm{E}}\mathrm{x}_3) + \dot{m}_4(\dot{\mathrm{E}}\mathrm{x}_4 - \dot{\mathrm{E}}\mathrm{x}_5), \tag{57}$$

$$\dot{\mathrm{E}}\mathrm{x}_{\mathrm{dest,r,HE}} = \dot{m}_7(\dot{\mathrm{E}}\mathrm{x}_8 - \dot{\mathrm{E}}\mathrm{x}_9 + \dot{\mathrm{E}}\mathrm{x}_{11} - \dot{\mathrm{E}}\mathrm{x}_{12}). \tag{58}$$

The exergetic coefficient of performance of the system for cooling and heating are as follows, respectively [60]:

$$\mathrm{COP}_{\mathrm{ex,h}} = \frac{\dot{Q}_{\mathrm{cond}}\left(1 - \frac{T_0}{T_{\mathrm{cond}}}\right) + \dot{Q}_{\mathrm{absor}}\left(1 - \frac{T_0}{T_{\mathrm{absor}}}\right)}{\dot{Q}_{\mathrm{g}}\left(1 - \frac{T_0}{T_{\mathrm{absor}}}\right) + \dot{W}_{\mathrm{pump,e}}}, \tag{59}$$

$$\mathrm{COP}_{\mathrm{ex,cool}} = \frac{\dot{Q}_{\mathrm{evap}}\left(1 - \frac{T_0}{T_{\mathrm{evap}}}\right)}{\dot{Q}_{\mathrm{g}}\left(1 - \frac{T_0}{T_{\mathrm{absor}}}\right) + \dot{W}_{\mathrm{pump,e}}}. \tag{60}$$

Sozen et al. [60] performed the performance tests of the system under the climate condition of Ankara in Turkey. A parabolic collector was installed to obtain required temperatures. In the experiments, high temperature water obtained from the collector was used as heat source needed for the generator. The system design configuration was analyzed by using the experimental data. The effect of irreversibilities in thermal process on the system performance in the system were determined. Thermodynamic analysis showed that both losses and irreversibility had an impact on absorption system performance, while potential for the improvement in the components of the system was determined. The components of the evaporator and absorber of the system had a higher exergy loss than the other components. In order to improve the performance of the system thermally, those components should be modified. Typical $\mathrm{COP}_{\mathrm{ex,h}}$ values of the system varied from 0.13 to 0.45. The highest and lowest $\mathrm{COP}_{\mathrm{ex,h}}$ values were obtained at higher evaporator temperature (10 °C) and the generator temperature of 75 °C, and at $T_{\mathrm{evap}} = 10$ °C and $T_{\mathrm{cond}} = 28$ °C, respectively.

Izquierdo et al. [61] studied on the entropy generated, the exergy destroyed and the exergetic efficiency of lithium-bromide absorption thermal compressors of single and double effect, driven by the heat supplied by a field of solar thermal collectors. A schematic of a single effect thermal compressor fed by a thermal collector is illustrated in Fig. 10 [61], where the solar cases heat storage system was not included. It consisted of an absorber, a desorber, the heat recoverer, the solution pump and the throttling valve. The compressor, driven by the heat produced by a field of solar collectors, absorbed the low pressure.

Izquierdo et al. [61] reported as follows: Two different applications, namely air-cooled and water-cooled units, were taken into account and compared with each other. Water-cooled compressors operated with temperatures and pressures lower than air-cooled compressors considering, in both cases, the same suction temperature, equal to 5 °C. While the absorption temperature in water-cooled compressors could reach 40 °C, in air-cooled systems it could vary between 30 °C and more than 50 °C. Under these conditions, the discharge temperature (boiling temperature within the desorber) of a single effect

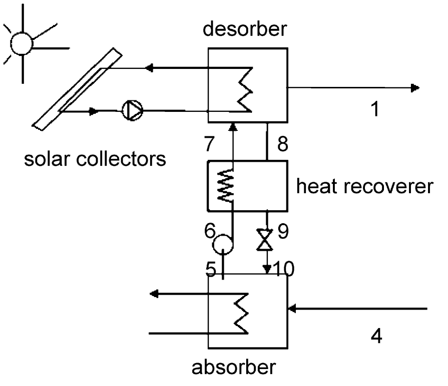


Fig. 10. Schematic of a single effect thermal compressor fed by a thermal collector drawn by Izquierdo et al. [61].

air-cooled unit ranged from 65 to 110 °C, while the maximum discharge pressure was around 0.12 bar. The discharge temperatures (boiling temperature within the high pressure desorber) of the double effect air-cooled thermal compressor varied from 110 °C for a final absorption temperature of 30–180 °C for a final absorption temperature of 50 °C. Discharge pressures could reach values of 0.3 and 1.5 bar, respectively. The lithium-bromide air-cooled thermal compressors of double-effect could be viable with absorption temperatures around 50 °C, when the temperature difference between the lithium-bromide solution and the outside air was about 8 °C. The exergetic efficiency of the air-cooled compressor of double effect was found to be 10% greater than the exergetic efficiency of the air-cooled thermal compressor of single effect. The exergetic efficiency of the air-cooled thermal compressor of double effect was also determined to be 10% higher than the exergetic efficiency of the water-cooled thermal compressor of single effect. The exergy of the solar radiation was better used by the air-cooled thermal compressor as the temperature of the external fluid feeding the high desorber was higher.

4.1.1.3.3. Adsorption units. Adsorption refrigeration is considered alternative to the conventional vapor compression refrigerator, especially in remote areas of the world without grid connected electricity. Activated carbon/methanol, activated carbon/ammonia, zeolite/water and silica gel/water are the adsorbent/adsorbate pairs commonly used in practically realized adsorption refrigeration cycles. A simple adsorption cycle indicating all the heat transfer for a complete cycle is shown in Fig. 11 [62]. Its principle of operation involves the processes of isosteric heating, desorption, isosteric cooling and resorption [62].

The thermodynamic efficiency (exergetic efficiency) relates the actual performance of a system to its expected maximum performance as determined from its ideal Carnot cycle. It may be written from a relation proposed by Pons et al. [63] as follows:

$$\varepsilon = \frac{\mathrm{COP_a}}{\mathrm{COP_{max}}} \tag{61}$$

with

$$\mathrm{COP_{max}} = \frac{1 - (T_{\mathrm{adsor}}/T_{\mathrm{g}})}{(T_{\mathrm{adsor}}/T_{\mathrm{evap}}) - 1} \tag{62}$$

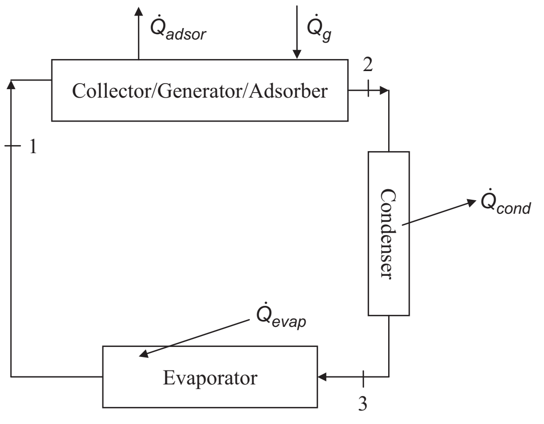


Fig. 11. Schematic of a simple adsorption refrigerator [62].

and

$$\mathrm{COP_a} = \frac{\dot{Q}_{\mathrm{evap}}}{\dot{Q}_{\mathrm{g}}}, \tag{63}$$

where $\dot{Q}_{\mathrm{evap}}$ and $\dot{Q}_{\mathrm{g}}$ are the heat transferred during refrigeration and the heat used to generate refrigerant during generation, respectively [62].

Anyanwu and Ogueke [62] reported as follows: The COP and thermodynamic efficiency depended on the mass of adsorbate generated and the generation temperature, T_{g}. Above a certain generator temperature, the mass of adsorbate generated was no longer a direct function of the temperature. In fact, in some cases, continued increase in generator temperature did not yield any adsorbate. Thus, an improved COP and consequently the thermodynamic efficiency would only come from an adsorbent that would readily desorb the adsorbate in its pores up to a low level of about 20–25 g of adsorbate per kg of adsorbent for the range of temperature obtainable using a conventional flat plate solar collector. This, however, was with the understanding that the refrigerant would have a high latent heat of vaporization. The activated carbon/ammonia for 0, −10 and −20 °C evaporator temperatures and 47 °C condenser temperature gave thermodynamic efficiency values above 100% at generator temperatures of about 70 °C. When the interest was air conditioning, the zeolite/water pair would be preferred while activated carbon/ammonia would be the preferred pair for other applications.

4.1.1.4. Solar cookers. Solar energy, which is an abundant, clean and safe source of energy, is an attractive to substitute for the conventional fuels for cooking [33]. In the literature, there are two studies conducted on the exergetic evaluation of the performance of solar cookers. A simply designed and the low-cost parabolic-type solar cooker (SPC) shown in Fig. 12 was made and tested by Ozturk [33]. He experimentally assessed the energy end exergy efficiencies of the cooker. Petela's analysis [32] was inspired by publication of Ozturk [33], in which for the first time the exergy efficiency was determined experimentally for the SPC of the cylindrical trough shape [32].

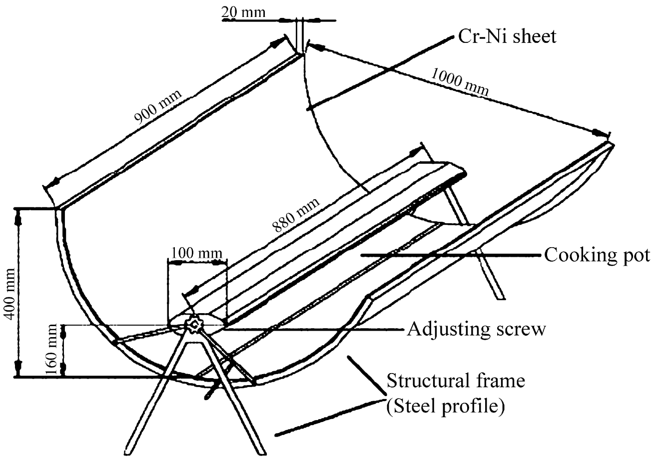


Fig. 12. A sketch of a solar parabolic cooker drawn by Ozturk [33].

The instantaneous exergy efficiency of the solar cooker can be defined as the ratio of the increased water exergy to the exergy of the solar radiation. Using Eqs. (21), (22) and (23b), it may be calculated as follows [33]:

$$\varepsilon_{\text{scook},1} = \frac{\dot{m}_{\text{w}} C_{\text{w}} \left[(T_{\text{w,out}} - T_{\text{w,in}}) - T_0 \left(\ln(T_{\text{w,out}}/T_{\text{w,in}}) \right) \right] / \Delta t}{I_{\text{T}} A_{\text{cook}} \left[1 + 1/3(T_0/T_{\text{s}})^4 - (4/3)(T_0/T_{\text{s}}) \right]}. \tag{64}$$

Exergy efficiency of the SPC was also defined by Petela [32] as the ratio of the exergy of the useful heat $\dot{Q}_{3u}$, at temperature T_3, and of the exergy of solar emission at temperature T_{s}. Using Eqs. (21), (22) and (24), it was proposed as follows [32]:

$$\varepsilon_{\text{scook},2} = \frac{\dot{Q}_{3\text{u}}(1 - (T_0/T_3))}{I_{\text{T}} \left[1 + 1/3(T_0/T_{\text{s}})^4 - (4/3)(T_0/T_{\text{s}}) \right]} \tag{65}$$

with the useful heat transferred through the wall of the cooking pot given by

$$\dot{Q}_{3\text{u}} = -A_3 U_3 (T_3 - T_{\text{w}}), \tag{66}$$

where T_3 is the absolute temperature of the surface 3, A_3 the outer surface area 3 of the cooking pot, U_3 the heat transfer coefficient (which takes into account the conductive heat transfer through the cooking pot wall and convective heat transfer from the inner cooking pot surface to the water) and T_{w} the absolute temperature of water in the cooking pot, as shown in Fig. 13 [32].

Fig. 12 illustrates the dimensions of a SPC, which was exergetically tested by Ozturk [33]. The overall dimensions of the SPC are $0.90 \times 1\,\text{m}^2$. The SPC was constructed of steel profile and Cr–Ni alloy sheet. Structural frame of the SPC, made of steel profile of dimensions $0.15 \times 0.15\,\text{m}^2$ and Cr–Ni alloy sheet, was screwed on the frame. The thickness of Cr–Ni sheet was 0.0005 m. In the center of the concentrating reflector, a cooking pot of 0.10 m width and 0.05 m in depth was welded. The cooking pot was made of galvanized steel sheet of 0.005 m thickness. All outer surfaces of the cooking pot were painted with mat black. There were no clouds so the reflector acted only on direct solar radiation. The reflector could be adjusted by means of the two screws on both sides of the cooking pot.

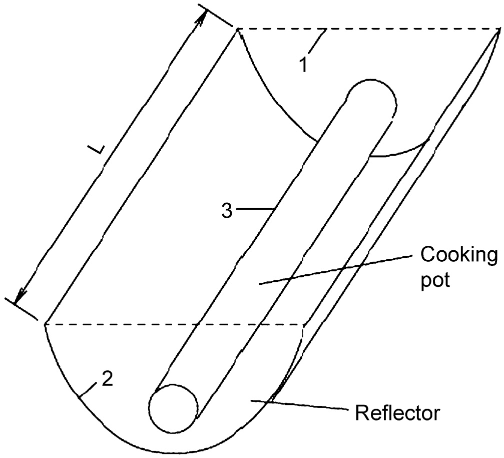


Fig. 13. A schematic of a solar parabolic cooker drawn by Petela [32].

The emissivity of the cooking pot and shield surfaces were 0.87 and 0.45, respectively [33]. Assumed were the following data: the time interval $\Delta t = 600\,\mathrm{s}$, the constant specific heat for water $C_\mathrm{w} = 4.2\,\mathrm{kJ/kg\,K}$ and the solar radiation temperature $T_\mathrm{s} = 6000\,\mathrm{K}$. The experimental time period was from 10:00 to 14:00 solar time. During this period, it was found that the daily average temperature of water in the SPC was 333 K and the daily average difference between the temperature of water in the cooking pot and the ambient air temperature was 31.6 K. The exergy output of the SPC varied between 2.9 and 6.6 W. The exergy efficiency of the SPC was obtained to range from 0.4% to 1.25% [33].

Petela [32] derived equations for heat transfer between the three surfaces: cooking pot, reflector and imagined surface making up the system. His model allowed for theoretical estimation of the energy and exergy losses: unabsorbed insolation, convective and radiative heat transfer to the ambient, and additionally, for the exergy losses: the radiative irreversibilities on the surfaces, and the irreversibility of the useful heat transferred to the water. The exergy efficiency of the SPC was found to be relatively very low (about 1%), and to be about 10 times smaller than the respective energy efficiency. The reasons for this were mainly due to the large exergy of the escaping insolation and additionally due to the degradation of the insolation absorbed on the surfaces of the reflector and the cooking pot. The theoretically calculated values of the efficiencies were relatively close to the values experimentally measured by Ozturk [33]. The influence of the input parameters (geometrical configuration, emissivities of the surfaces, heat transfer coefficients and temperatures of water and ambience) was also determined on the output parameters, the distribution of the energy and exergy losses and the respective efficiencies [32].

4.1.1.5. Industrial process heat. Cylindrical parabolic collector systems look very promising for delivering industrial process heat applications in 95–350 °C delivery temperature range [41]. In this regard, Eskin [42] made a simulation study on a solar process heat system shown in Fig. 14 [41], validated by experimental results and represented the unsteady performance analysis of this system. She also evaluated exergetic

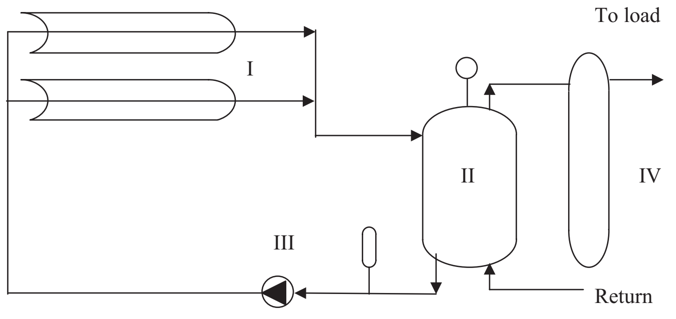


Fig. 14. A schematic view of the solar process heating system [41] (I: cylindrical parabolic collector array, II: storage tank, III: circulating pump, IV: auxiliary heater).

performance of the particular systems, while her analysis considered the unsteady-state thermal and exergetic assessment of the collector and the storage tank individually.

The exergy efficiency of the cylindrical parabolic solar collector was calculated as follows:

$$\varepsilon_{\text{par,col}} = 1 - \frac{\dot{I}_{\text{par,col}}}{\dot{\text{E}}\text{x}_{\text{par,s}}} \tag{67}$$

with

$$\text{E}\dot{\text{x}}_{\text{par,s}} = A\psi_{\text{srad,be,d}}. \tag{68}$$

The auxiliary heater in the system eliminated the difference between energy demand and solar energy harvesting. When the temperature of the water entering the load fell below the predetermined temperature level, the auxiliary heater was activated. The simulation results indicated that the exergetic efficiency (at a maximal value of about 37%) was highly dependent on the ratio of mass flow rates and the use of an auxiliary heater in the system.

4.1.1.6. Solar desalination systems. There are very limited studies on the exergetic evaluation of solar desalination systems in the open literature. The Spanish research institution, Centro de Investigaciones Energtticas, Medioambientales y Tecnologicas and the German Deutsche Forschungsanstalt fur Luft- und Raumfahrt e.V. decided in 1987 to develop a solar thermal desalination project at the Plataforma Solar de Almeria. In July, 1988, the first start-up of a solar multi-effect distillation system took place at the Plataforma Solar de Aimeria, a solar research centre located in southeastern Spain, near Aimeria. Its evaluation was finished in December, 1990. The plant, known as "So1-14" was built and connected to the previous existing solar facilities as a result of a Spanish–German project [64]. The performance of this solar desalination system was evaluated by Garcia-Rodriguez and Gomez-Camacho [64] using energy and exergy analysis method in order to propose possible improvements of the system, as presented partly below.

In the exergetic analysis of the system indicated in Fig. 15 [64], Eq. (15) was used and the results obtained on a component basis are listed in Table 3 [64]. It is obvious that solar multi-effect distillation with 14 cells had the lowest exergetic efficiency, while the thermal storage had the highest one.

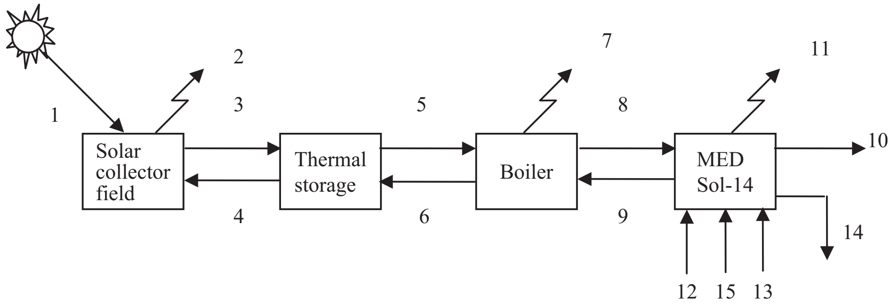


Fig. 15. Solar multi-effect distillation (MED) system at Phase I of the solar thermal desalination project [64]. (1) Solar input, (2) optic and thermal losses, (3–6) synthetic oils at various temperatures, (7) thermal losses, (8) saturated steam, (9) saturated water, (10) fresh water (product), (11) thermal losses, (12) seawater, (13) cooling outlet stream, (14) blowdown and (15) auxiliary power consumption.

Table 3
Exergetic performance of the equipment at Phase I of the solar thermal desalination project [64]

Equipment	$\dot{F}$ (kW)	$\dot{P}$ (kW)	$\dot{F}-\dot{P}$ (kW)	$\varepsilon = \dot{P}/\dot{F}$ (%)
Solar collector	336.9	58.63	278.3	17.4
Thermal storage	58.63	≅58.63	≅0	≅100
Boiler	58.63	26.21	32.42	44.7
Solar multi-effect distillation (MED)	34.91	4.992	29.92	14.3
Global system	345.6	4.992	340.6	1.4

4.1.1.7. Solar thermal power plants. The solar thermal power system in general can be considered as consisting of two subsystems, namely, the collector–receiver subsystem and heat engine subsystem as illustrated in Fig. 16 [12]. The collector–receiver circuit consists of a number of parabolic trough collectors arranged in modules operating in tracking mode. The main components of the heat engine circuit are a heater (here the boiler heat exchanger), a turbine having two stages, a condenser, pump and a regenerator. Exergy analysis is conducted in two main subsystems along with their components, as given by Singh et al. [12].

The overall exergy efficiency of the collector–receiver circuit is calculated in a similar manner given by Eq. (22) as follows [12]:

$$\varepsilon_{\text{o,col-rec}} = \frac{\text{E}\dot{\text{x}}_{\text{u,col-rec}}}{\text{E}\dot{\text{x}}_{\text{par,s}}} \tag{69}$$

with the useful exergy of the whole parabolic collector

$$\text{E}\dot{\text{x}}_{\text{u,col-rec}} = n_{\text{par,col}}\text{E}\dot{\text{x}}_{\text{u}} \tag{70}$$

and the exergy received by the parabolic collector given as:

$$\text{E}\dot{\text{x}}_{\text{par,s}} = \dot{Q}_{\text{s}}\left(1 - \frac{T_0}{T_{\text{s}}}\right), \tag{71}$$

where $n_{\text{par,col}}$ is the number of the parabolic collectors, $\dot{Q}_{\text{s}}$ is the transferred solar heat and T_{s} is the solar temperature. The exergy received by the parabolic collector may also be

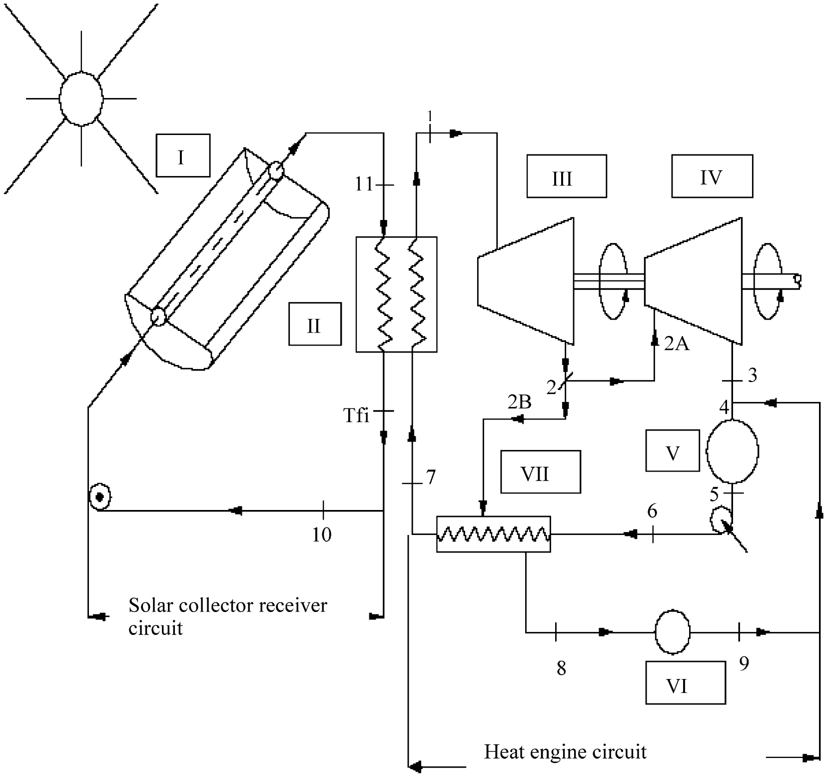


Fig. 16. Schematic of a solar power thermal plant drawn by Singh et al. [12]. (I) Parabolic through collector, (II) boiler heat exchanger, (III) high-pressure turbine, (IV) low-pressure turbine, (V) condenser, (VI) valve, (VII) regenerator.

calculated using Eqs. (25)–(26), and the relations given in Table 1. The useful exergy of the one parabolic collector ($\dot{Ex}_u$) may be found using Eq. (23b) or (23c).

The total efficiency of the heat engine subsystem consisting of the boiler heat exchanger and the heat engine cycle is calculated as follows:

$$\varepsilon_{h,eng} = \frac{\dot{W}_{net}}{\dot{Ex}_{h,eng}} \tag{72}$$

with the available exergy of the working fluid of the heat engine cycle given as:

$$\dot{Ex}_{h,eng} = \dot{Q}_u\left(1 - \frac{T_0}{T_{Ran,0}}\right), \tag{73}$$

where $\dot{Q}_u$ is the useful transferred heat, $\dot{W}_{net}$ is the net work done by the heat engine cycle and $T_{Ran,0}$ is the ambient temperature of the Rankine cycle [12].

The overall exergy efficiency of the solar thermal power system is the product of the two separate efficiencies of the subsystems, as given below [12]:

$$\varepsilon_{h,eng} = \frac{\dot{W}_{net}}{\dot{Ex}_{par,s}}. \tag{74}$$

You and Hu [65] investigated the optimal thermal and exergetic efficiencies of a medium-temperature solar thermal power system using energy and exergy analysis method. A simple reheat-regenerative arrangement is schematically shown in Fig. 17 [65].

The exergetic efficiency of the cycle (including the exergy loss in the heating process) is as follows [65]:

$$\varepsilon_{\text{cycle}} = \frac{\dot{W}_{\text{turbine}}}{\text{E}\dot{\text{x}}_{\text{Q}}}. \tag{75}$$

$\text{E}\dot{\text{x}}_{\text{Q}}$ is calculated using Eq. (23c) where $T_{\text{w,out}}$ and $T_{\text{w,out}}$ are the temperatures of the solar heat carrier entering and exiting the heat exchanger(s), respectively.

The exergetic efficiency of the collector is calculated from [65]:

$$\varepsilon_{\text{par,s}} = \frac{\text{E}\dot{\text{x}}_{\text{Q}}}{\text{E}\dot{\text{x}}_{\text{s}}} \tag{76}$$

with

$$\text{E}\dot{\text{x}}_{\text{s}} = I_{\text{T}}\left[1 - \frac{4}{3}\frac{T_{\text{am}}}{T_{\text{s}}}(1 - 0.28f)\right]. \tag{77}$$

The overall exergy efficiency of the combined system of the collector and the power cycle is the product of the two separate efficiencies of the subsystems, as given by the equation [65].

$$\varepsilon_{\text{sys}} = \varepsilon_{\text{cycle}}\varepsilon_{\text{par,s}}. \tag{78}$$

Singh et al. [12] calculated the irreversibilities of the solar thermal power plant illustrated in Fig. 16 [12]. It was found that the collector and receiver had the highest irreversibilities and the efforts to reduce exergy loss should be made in this assembly. The component exergy efficiency values were as follows: Collector: 29.03%, receiver: 68.38%, collector–receiver: 19.85%, boiler heat exchanger: 96.42%, heat engine: 66.57% and overall system: 12.74%.

You and Hu [65] reported based their analysis that the reheat-regenerative arrangement was suitable for the medium-temperature solar thermal power generation purpose. There

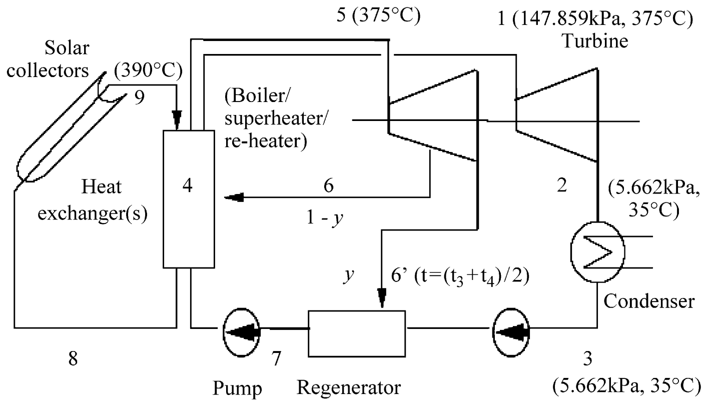


Fig. 17. Schematic of one-stage reheat-regenerative power cycle and the parabolic trough collector drawn by You and Hu [65].

was an optimum saturation temperature in the boiler or an optimum temperature the fluid entering the solar field (with the same exiting temperature) at which both the thermal efficiency and the exergetic efficiency of the combined system of the reheat-regenerative cycle and the solar collector hit the maximum values simultaneously.

4.1.2. Photovoltaics

Exergetic evaluation of PVs has been performed by some investigators [66,67] in hybrid (PV/thermal) systems as a part of the system. This evaluation is explained in Section 4.1.3 in more detail.

Electrical energy is not affected by ambient conditions and therefore is equivalent in work. If global irradiance is I, energetic efficiency of the solar cell is η_{scell}, the instantaneous electrical exergy is then as follows [66].

$$\mathrm{E\dot{x}_e} = \eta_{\mathrm{scell}} I = \varepsilon_{\mathrm{scell}} I, \tag{79}$$

where $\varepsilon_{\mathrm{scell}}$ is the exergetic efficiency of the solar cell.

4.1.3. Hybrid (PV/thermal) solar collectors

The exergy efficiency of a hybrid solar collector, that generates both electric power and heat, may be calculated as follows [67].

$$\varepsilon_{\mathrm{PV/Thermal}} = \frac{\eta_{\mathrm{conver}} I + \mathrm{E\dot{x}_{solar}}}{\mathrm{E\dot{x}_I}} \tag{80}$$

with

$$\mathrm{E\dot{x}_{solar}} = \frac{T_{\mathrm{fluid}} - T_0}{T_{\mathrm{fluid}}} \dot{Q}_{\mathrm{solar}} \tag{81}$$

and

$$\mathrm{E\dot{x}_I} = 0.95 I, \tag{82}$$

where η_{conver} is the conversion efficiency, I the global irradiance (W/m^2), $\mathrm{E\dot{x}_{solar}}$ the exergy of heat (W/m^2), $\mathrm{E\dot{x}_I}$ the exergy of global irradiance (W/m^2), $\dot{Q}_{\mathrm{solar}}$ the collected solar heat amount per unit time per panel area (W/m^2) and T_{fluid} the supply temperature of collector fluid (K).

Fujisawa and Tani [66] defined the s*ynthetic exergy of the PV/T collector as* the total value of the electrical and thermal exergies as follows:

$$\mathrm{E\dot{x}_{PV/T}} = \mathrm{E\dot{x}_e} + \mathrm{E\dot{x}_{thermal}} = (\varepsilon_e + \varepsilon_{\mathrm{thermal}}) = \varepsilon_{\mathrm{PV/T}} I \tag{83}$$

with

$$\mathrm{E\dot{x}_e} = \varepsilon_e I \tag{84}$$

and

$$\mathrm{E\dot{x}_{thermal}} = \dot{Q}\eta_{\mathrm{Carnot}} = \dot{Q}\left(\frac{T_f - T_0}{T_f}\right) = \varepsilon_{\mathrm{thermal}} I. \tag{85}$$

Fujisawa and Tani [66] designed and constructed a PV-thermal hybrid collector on their campus. The collector consisted of a liquid heating fiat-plate solar collector with mono-Si PV cells on substrate of non-selective aluminum absorber plate, The collector area was $1.3 \times 0.5\,\mathrm{m}^2$. From the annual experimental evaluation based on exergy, Fujisawa and Tani

concluded that the PV/T collector could produce higher output density than a unit PV module or liquid heating fiat-plate solar collector. Using exergetic evaluation, the best performance of available energy was found to be that of the coverless PV/T collector at 80.8 kWh/yr, the second to be the PV module at 72.6 kWh/yr, the third to be the single-covered PV/T collector at 71.5 kWh/yr, and the worst to be the flat-plate collector at 6.0 kW h/yr.

Saitoh et al. [67] performed field measurements from November 1998 to October 1999 at a low energy house at Hokkaido University. A system diagram of the experimental equipment is illustrated in Fig. 18 [67]. The power generated was measured by giving the variable load for the maximum power point tracking. Two hybrid solar panels were connected in parallel, while the brine was supplied at constant temperature by a fluid supply system with a circulating pump. The volumetric flow rate per panel was fixed at 1 l/min. The tilt angle of the panel was 30°, which gave the maximum annual global irradiance. Except for winter, the mean conversion efficiency of array and the collector efficiency were stable at 8–9% and 25–28%, respectively. The dependency on solar energy was 46.3%. Energy and exergy efficiency values of single-junction crystalline silicon PV are illustrated in Table 4 [67]. The exergy efficiencies of solar collector, PV and hybrid solar collector were found to be 4.4%, 11.2% and 13.3%, respectively. Solar collector had the lowest value. In terms of energy quality, the hybrid solar collector was very effective [67].

4.2. Wind energy systems

The exergy of fluid currents is entirely due to the kinetic energy of the fluid. The maximum work is extracted from a moving fluid when the velocity is brought to zero relative to the reference state. The kinetic energy of the fluid and its exergy have the same numerical value [14].

$$\psi_{\text{fluid}} = \frac{1}{2}\rho V_0^3, \tag{86}$$

where ρ is the density of the wind and V_0 is the wind speed.

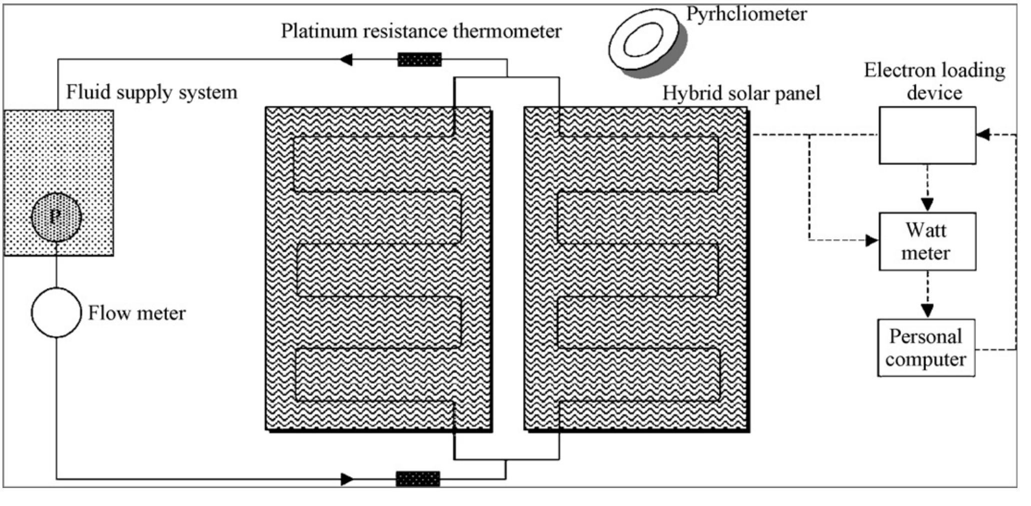


Fig. 18. System diagram of experimental equipment drawn by Saitoh et al. [67].

Table 4
Comparison of energy and exergy efficiency values of solar collector, photovoltaic and hybrid collector [67]

Type of efficiency	Solar collector	Photovoltaic	Hybrid collector
Energy efficiency (η, %)			
Heat	46.2	—	32.0
Power	—	10.7	10.6
Total	46.2	10.7	42.6
Exergy efficiency (ε, %)			
Heat	4.4	—	2.1
Power	—	11.2	11.2
Total	4.4	11.2	13.3

Koroneos et al. [11] presented two diagrams where utilization of the wind's potential in relation to the wind speed and exergy losses in the different components of a wind turbine (i.e., rotor, gearbox and generator) were included. They concluded as follows: "According to Betz's law, wind turbine can take advantage of up to 60% of the power of the wind. Nevertheless, in practice, their efficiency is about 40% for quite high wind speeds. The rest of the energy density of the wind not obtainable is exergy loss. This exergy loss appears mainly as heat. It is attributed to the friction between the rotor shaft and the bearings, the heat that the cooling fluid abducts from the gearbox, the heat that the cooling fluid of the generator abducts from it and the thyristors, which assist in smooth starting of the turbine and which lose 1–2% of the energy that passes through them."

As for as studies conducted on exergetic assessment of wind energy systems, Sahin et al. [68] developed a new exergy formulation for wind energy, which was more realistic and also accounted for the thermodynamic quantities enthalpy and entropy. The relation developed for the total exergy for wind energy is as follows, while the input and output variables for the system considered are illustrated in Fig. 19 [68].

$$\mathrm{E\dot{x}} = \dot{E}_{\mathrm{gen}} + \dot{m}C_{\mathrm{p}}(T_2 - T_1) + \dot{m}T_{\mathrm{at}}\left(C_{\mathrm{p}}\ln\frac{T_2}{T_1} - R\ln\frac{P_2}{P_1} - \frac{\dot{Q}_{\mathrm{loss}}}{T_{\mathrm{at}}}\right) \quad (87)$$

with

$$\dot{Q}_{\mathrm{loss}} = \dot{m}C_{\mathrm{p}}(T_{\mathrm{at}} - T_{\mathrm{ave}}), \quad (88)$$

where $\dot{E}_{\mathrm{gen}}$ is the generated electricity (i.e., the total kinetic energy difference), T_{at} is the atmospheric temperature, P_2 is the pressure at the exit of the wind turbine for a wind speed V_2 and P_1 is the pressure at the inlet of the wind turbine for a wind speed V_1, $\dot{Q}_{\mathrm{loss}}$ represents heat losses of wind turbine and T_{ave} is the mean value of input and output wind chill temperatures.

Sahin et al. [68] reported as follows: "The exergy analysis of wind energy shows that there are significant differences between energy and exergy analysis results. According to one classical wind energy efficiency analysis technique, which examines capacity factor, the resultant wind energy efficiency is overestimated relative to what it really is. The capacity factor normally refers to the percentage of nominal power that the wind turbine generates. Average differences between energy and exergy efficiencies are approximately 40% at low wind speeds and up to approximately 55% at high wind speeds".

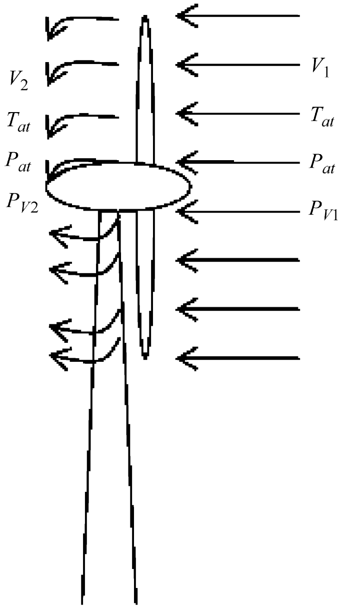


Fig. 19. Wind turbine and representative wind energy input and output variables drawn by Sahin et al. [68].

Ozgener and Ozgener [69] performed exergy analysis of a wind turbine system (1.5 kW) located in Solar Energy Institute of Ege University (latitude 38.24N, longitude 27.50E), Izmir, Turkey. They reported that exergy efficiency changed between 0% and 48.7% at different wind speeds based on a dead state temperature of 25 °C and a atmospheric pressure of 101.325 kPa, considering pressure differences between state points. Depending on temperature differences between state points, exergy efficiencies were found to be 0–89%.

The exergetic efficiency of a turbine is defined as a measure of how well the stream exergy of the fluid is converted into useful turbine work output or inverter work output. By using inverter work output as useful work and applying this to wind turbine, the following relations are obtained [69].

$$\varepsilon = \frac{\dot{W}_{\mathrm{e,io}}}{\dot{\mathrm{Ex}}_1 - \dot{\mathrm{Ex}}_2} \tag{89}$$

with

$$\dot{\mathrm{Ex}}_{\mathrm{dest}} = (\dot{\mathrm{Ex}}_1 - \dot{\mathrm{Ex}}_2) - \dot{W}_{\mathrm{e}}, \tag{90}$$

where $\dot{W}_{\mathrm{e,io}}$ is the power at inverter output and $\dot{\mathrm{Ex}}_{\mathrm{dest}}$ is the exergy destruction, while $\dot{\mathrm{Ex}}_1$ and $\dot{\mathrm{Ex}}_2$ are exergy rates calculated using Eqs. (12) and (13).

4.3. Geothermal energy systems

The specific exergy of a geothermal site depends on the temperature at the collector, the pressure and composition of fluid in the reservoir, and the ability of the surrounding rock or fluid to transport thermal energy to the collector. Utilization of a geothermal site often

changes the thermal or fluid properties of the reservoir to a new equilibrium dependent on the method of energy extraction [14].

4.3.1. Classification of geothermal resources by exergy

Geothermal resources have been classified as low, intermediate or high enthalpy resources according to their reservoir temperatures. The temperature ranges used for these classifications are arbitrary and they are not generally agreed upon. Temperature is used as the classification parameter because it is the earliest to measure and understand. In addition, temperature or enthalpy alone can be ambiguous defining a geothermal resource because two independent thermodynamic properties are required to define the thermodynamic state of fluid. Geothermal energy is already in the form of heat, and from the thermodynamic point of view, work is more useful than heat because not all the heat can be converted to work. Therefore, geothermal resources should be classified by their exergy, a measure of their ability to do work [70,71].

Lee [71] proposed a new parameter, the so-called specific exergy index (SExI) for better classification and evaluation as follows:

$$\mathrm{SExI} = \frac{h_{\mathrm{brine}} - 273.16 s_{\mathrm{brine}}}{1192}, \tag{91}$$

which is a straight line on an $h{-}s$ plot of the Mollier diagram. Straight lines of SExI $= 0.5$ and SExI $= 0.05$ can therefore be drawn in this diagram and used as a map for classifying geothermal resources by taking into account the following criteria:

- SExI <0.05 for low-quality geothermal resources,
- $0.05 \leqslant$ SExI < 0.5 for medium-quality geothermal resources, and
- SExI $\geqslant 0.5$ for high-quality geothermal resources.

Here, the demarcation limits for these indices are exergies of saturated water and dry saturated steam at 1 bar absolute.

In order to map any geothermal field on the Mollier diagram as well as to determine the energy and exergy values of the geothermal brine, the average values for the enthalpy and entropy are then calculated from the following equations [72]:

$$h_{\mathrm{brine}} = \frac{\sum_i^n \dot{m}_{w,i} h_{w,i}}{\sum_i^n \dot{m}_{w,i}}, \tag{92}$$

$$s_{\mathrm{brine}} = \frac{\sum_i^n \dot{m}_{w,i} s_{w,i}}{\sum_i^n \dot{m}_{w,i}}. \tag{93}$$

The above classification has been used by some investigators in their studies. In this regard, Quijano [72] performed exergy analysis of the Ahuachapán and Berlín geothermal fields. Plotting the thermodynamic conditions of both fields on the Molliere diagram and computing the specific exergy index (SEI), the fields were classified on the medium high exergy zone. Ozgener et al. [73] and Baba et al. [74] applied the SExI to the Balcova geothermal field, which is located in the western part of Turkey, and is endowed with considerably rich geothermal resources. The number of the wells in operation in this field may vary depending on the heating days and operating strategy. Taking into account the eight productive wells, which were in operation at the date considered and using Eq. (91)

together with the values given in Table 5 [74], the SExI was found to be 0.07. This represented that the field fell into the medium quality geothermal resources according to the classification of Lee [71]. For classifying the Balcova geothermal field according to its reservoir, the weighted average value of the temperature (T_{brine}) was obtained to be 113.9 °C by using the similar relation given in Eq. (91). This field fell into the intermediate enthalpy resources according to the classifications of Muffler and Cataldi [75] and Benderitter and Cormy [76], while it is characterized as low enthalpy resources according to the classification of Hochstein [77]. This clearly indicated that the classification with reference to SExI was more meaningful as there was no general agreement on the arbitrary temperature ranges used in the classification of geothermal resources by temperature. Ozgener et al. [78,79] also determined the SExI values for the Gonen and Salihli geothermal fields in Turkey as 0.025 and 0.049, respectively. They concluded that both these fields fell into the low quality geothermal resources according to the classification of Lee. Etemoglu and Can [80] classified geothermal resources in Turkey based on SExI. In their analysis, the triple point of water was selected as the dead-state conditions since the enthalpy and entropy values were zero. SExI values of geothermal resources over 0.56 were classified as high exergy resources, SER $<$ 0.05 low exergy and between of these values were medium exergy resources.

4.3.2. Direct utilization

4.3.2.1. District heating. Although various studies have been undertaken to perform energy and exergy analyses of geothermal systems, the exergy analysis of geothermal district heating systems (GDHSs) based on the actual data was performed by Ozgener et al. [81] for the first time (to the best of authors' knowledge). In this context, the first study included a comprehensive energy and exergy analysis conducted on the Balcova geothermal district heating system located in the town Balcova, Izmir, Turkey, using actual data sets obtained as of January 1, 2003 for system analysis, performance evaluation and efficiency improvement. Since then, Ozgener et al. have conducted various studies on exergetic [82,83] and exergoeconomic analyses [84,85] of GDHSs, namely Balcova, Salihli and Gonen GDHSs installed in the provinces of Izmir, Manisa and Balikesir, Turkey

Table 5
Some thermodynamic properties of the wells in the Balcova geothermal field in Izmir, Turkey (as of 1 January 2003) [74]

Code of well	Temperature T (°C)	Mass flow rate $\dot{m}$ (kg/s)	Pressure P (kPa)	Specific enthalpy h (kJ/kg)	Specific entropy s (kJ/kg K)
BD2	131.6	18.31	413.4	552.98	1.6507
BD3	120	18.65	522.83	503.72	1.5270
BD4	135	25.32	539.04	567.57	1.6863
BD5	111.4	3.74	607.95	467.35	1.4333
BD7	110.6	20.01	496.49	463.89	1.4245
B4	98.8	13.16	368.81	413.99	1.2926
B5	103.6	23.10	332.34	434.20	1.3467
B10	96	25.90	364.76	402.19	1.2607
BD8 (reinjection)	66.1	112.02	474.20	276.8	0.9061
Average values	113.9	148.19	—	477.87	1.4578

as well as on investigating the effect of dead state temperature on the energy and exergy efficiencies of GDHSs [86,87]. They also performed a key review on the performance improvement aspects of GDHSs [88] and prepared a general paper on geothermal energy including the exergetic evaluation of GDHSs for the Encyclopedia of Energy Engineering [89].

The following relations have been summarized from the previous studies performed by Ozgener et al. [81–91] as follows:

A schematic diagram of the simplified GDHS, where user system is heated by geothermal energy, is illustrated in Fig. 20 [88]. As can be seen in this figure, a GDHS consists mainly of three circuits, namely (a) energy production circuit (EPC; geothermal well loop), (b) energy distribution circuit (EDC; district heating distribution network, and (c) energy consumption circuit (ECC). In evaluating the system performance from the exergetic point of view, the two items of the whole system play a big role. These include: (i) the geothermal brine exergy inputs from the production field and (ii) exergy destructions in the system taking place as the exergy of the fluid lost in the heat exchanger, the natural direct discharge of the system (pipeline losses), and the pumps.

For a general steady-state, steady-flow process, the two balance equations, namely mass and exergy balance equations, may be written as follows:

Using Eq. (1), the mass balance equations for two various GDHSs, namely GDHSs with reinjected thermal water (i.e., Balcova GDHS) and without reinjected thermal water (i.e., Salihli GDHS), may be written as follows, respectively [88]:

$$\sum_{i=1}^{n} \dot{m}_{\mathrm{w,T}} - \dot{m}_{\mathrm{r}} - \dot{m}_{\mathrm{d}} = 0 \tag{94}$$

and

$$\sum_{i=1}^{n} \dot{m}_{\mathrm{w,T}} - \dot{m}_{\mathrm{d}} = 0, \tag{95}$$

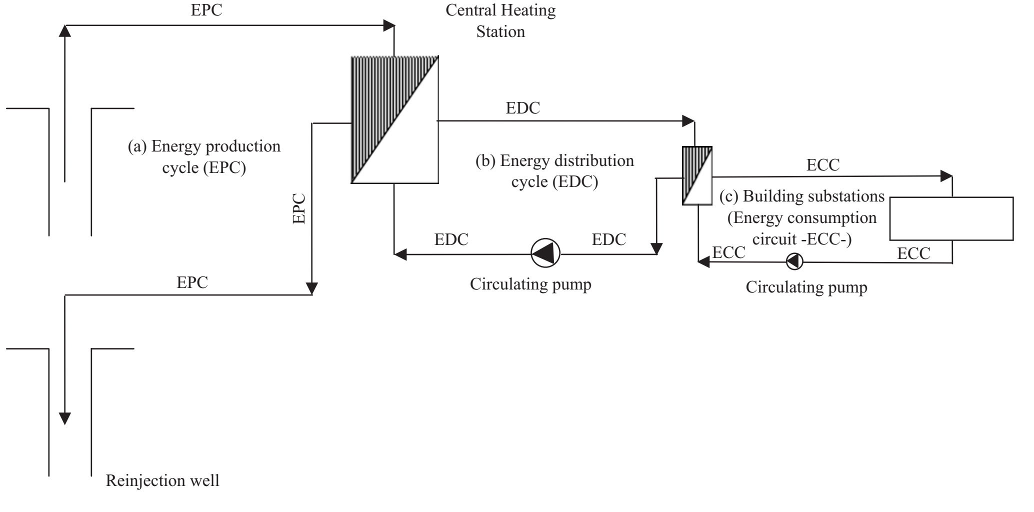


Fig. 20. Basic simplified geothermal district heating energy system schema [90].

where $\dot{m}_{w,T}$ is the total mass flow rate at wellhead, $\dot{m}_r$ is the flow rate of the reinjected thermal water and $\dot{m}_d$ is the mass flow rate of the natural direct discharge.

The exergy destructions in the heat exchanger, pump and the system itself are calculated as follows [88]:

$$\dot{E}x_{dest,HE} = \dot{E}x_{in} - \dot{E}x_{out} = \dot{E}x_{dest}, \tag{96}$$

$$\dot{E}x_{dest,pump} = \dot{W}_{pump} - \left(\dot{E}x_{out} - \dot{E}x_{in}\right) \tag{97}$$

and

$$\dot{E}x_{dest,system} = \sum \dot{E}x_{dest,HE} + \sum \dot{E}x_{dest,pump}. \tag{98}$$

Using Eq. (15), the exergy efficiencies of two various GDHSs with reinjected thermal water and without reinjected thermal water are found from the following relations, respectively [88].

$$\varepsilon_{GDHS,wr} = \frac{\dot{E}x_{useful,HE}}{\dot{E}x_{brine}} = 1 - \frac{\dot{E}x_{dest,system} + \dot{E}x_{reinjected} + \dot{E}x_{natural\ discharged}}{\dot{E}x_{brine}}, \tag{99}$$

$$\varepsilon_{GDHS,wor} = \frac{\dot{E}x_{useful,HE}}{\dot{E}x_{brine}} = 1 - \frac{\dot{E}x_{dest,system} + \dot{E}x_{natural\ discharged}}{\dot{E}x_{brine}}, \tag{100}$$

where $\dot{E}x_{dest,system}$ is the exergy destructions in the system taking place as the exergy of the fluid lost in the heat exchanger and the pumps, $\dot{E}x_{reinjected}$ is the exergy loss due to the reinjected water and $\dot{E}x_{natural\ discharged}$ is the exergy destruction due to the natural direct discharge of the system (due to a significant amount of water leaks; pipeline losses).

Table 6 [81–83,86,87,90,91] shows a comparison of exergy efficiency values for GDHSs installed in Turkey. As can be seen in this table, exergy efficiencies range from 42.94% to 66.13% depending on the various dead state temperatures. As expected, the lower the reference state temperature, the significantly larger the exergy losses in the system pipeline and heat exchangers. However, exergy rates of pipeline losses of the system, heat exchangers, and useful exergy increase considerably. The reason for this rapid rise in exergy rates is due to a decrease in the ambient temperature [88].

Ozgener et al. [88] also studied on the effect of varying dead state temperatures on the exergy efficiencies of the whole GDHS. Exergy efficiency values were correlated with high correlation coefficients for the Balcova, Gonen and Salihli GDHSs. Of these, the correlation for the Balcova GDHS is given below [87]

$$\varepsilon_{Balcova,\ GDHS} = 0.000006 - 0.00005T_{am}^3 - 0.1279T_{am} + 45.21, \tag{101}$$

where T_{am} is the ambient temperature in °C.

4.3.2.2. Ground-source (geothermal) heat pumps. Ground-source heat pumps (GSHPs) have been used for years in the developed countries due to their higher energy utilization efficiencies compared with conventional heating and cooling systems. There are two main types of GSHP system. (a) ground-coupled (vertical or horizontal)-closed loop and (b) water source-open loop. Ground-coupled heat pumps are known by a variety of names. These include GSHPs, earth-coupled heat pumps, earth energy heat pumping systems, earth energy systems, ground-source systems, geothermal heat pumps, closed-loop heat

Table 6
Comparison of various geothermal district heating systems in terms of exergy destructions and exergy efficiencies [81–83,90,91,86,87]

Name of GDHS	Location/ country	Dead state temperature (°C)	Date of data used	Total exergy input (kW)	Exergy destructions/losses (% of the total (brine) exergy input)				Exergy efficiency (%)	References
					Pumps	Heat exchangers	Thermal reinjection	Natural direct discharge (pipe line)		
Balcova GDHS	Izmir/Turkey	13.1	1 January 2003	9164.29	3.22	7.24	22.66	24.1	42.94	[81]
Gonen GDHS	Balikesir/ Turkey	6	1 February 2004	2657.5	14.81	7.11	12.96	1.06	64.06	[82]
Salihli GDHS	Manisa/ Turkey	2.9	1 February 2004	2564	2.22	17.90	—	20.44	59.44	[83]
Balcova GDHS	Izmir/Turkey	13.1[a]	2 January 2004	14808.15	1.64	8.57	14.84	28.96	46.00	[84]
Gonen GDHS	Balikesir/ Turkey	10[b]	1 February 2004	2333.33	17.45	8.19	7.37	0.86	66.13	[85]
Salihli GDHS	Manisa/ Turkey	25[c]	1 February 2004	1524	4.27	31.17	—	8.98	55.58	[88]
Balcova GDHS	Izmir/Turkey	11.4[d]	2 January 2004	14390	1.74	8.83	14.18	28.7	46.55	[89]

[a]The study was conducted for four various dates , namely 1 January 2003 , 2 December 2003, 2 January 2004 and 2 February 2004 at dead state temperatures of 13.1, 12, 10.4 and 6.5 °C, respectively.

[b]A parametric study was performed o investigate how varying reference how varying reference temperature from 0 to 20 °C would affect the exergy efficiencies.

[c]The study was conducted for 1 December 2003, 1 January 2004 and 1 February 2004 at dead state temperatures of 10.8, 9.7 and 2.9, respectively. In addition, two parametric expressions of exergy efficiencies were developed as a function of the reference temperature, by varying the dead state temperature from 0 to 25 °C.

[d]The reference-state temperature value of 11.4 °C was obtained from the average ambient temperature data measured between 2000 and 2004 for second January in Izmir. The dead state temperature was considered varying from 0 to 25 °C to conduct a parametric study.

pumps, solar energy heat pumps, geoexchange systems, geosource heat pumps, and a few other variations [92].

Fig. 21 [93] illustrates a schematic diagram of a GSHP system in the heating mode as an illustrative example. The system was designed and installed in the Solar Energy Institute of Ege University, Izmir, Turkey. The system was commissioned in May 2000, while GSHP systems have been applied to the Turkish residential buildings since 1997.

The performance tests have also been performed since then. This system has been recently integrated with a solar collector and a greenhouse [94]. It mainly consists of three separate circuits: (i) the ground coupling circuit (brine circuit or water-antifreeze solution circuit), (ii) the refrigerant circuit (or a reversible vapor compression cycle) and (iii) the fan coil circuit (water circuit).

In Table 7 [95], Eqs. (102)–(126) used in modeling and analyzing GSHP systems are summarized [95]. These relations have been obtained for each of the GSHP components illustrated in Fig. 21 using mass, energy, entropy and exergy balance equations as well as the exergy destructions obtained using exergy balance equations given in Section 3).

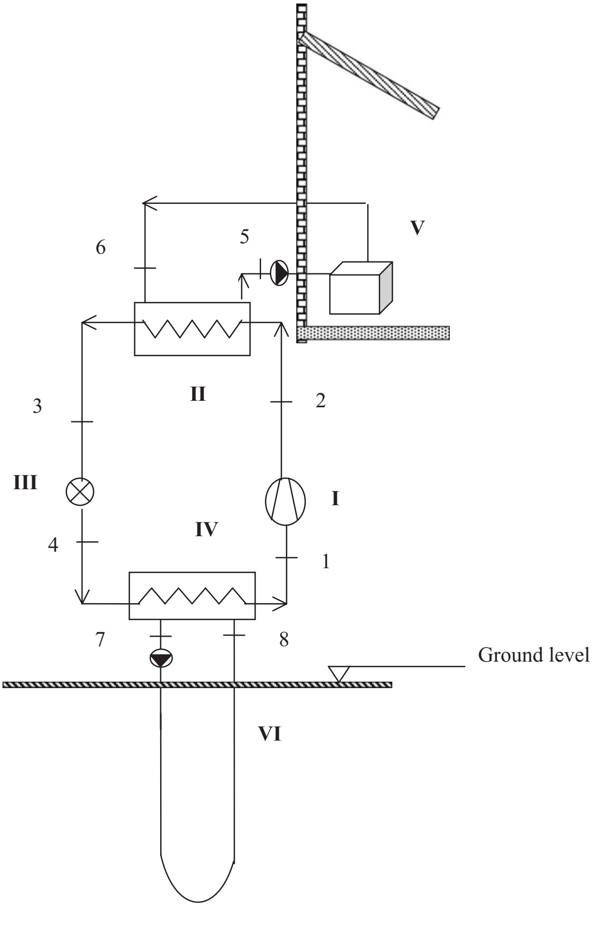


Fig. 21. The main components and schematic of a ground-source heat pump system [93]. (I) Compressor, (II) condenser, (III) capillary tube, (IV) evaporator, (V) fan-coil unit, (VI) ground heat exchanger.

Table 7
Mass, energy, exergy and entropy balance relations of a GSHP system [95]

No	Element	Mass analysis using Eq. (1) (the conversion of mass principle)	The irreversibility or the exergy destroyed using Eq. (5a) (the exergy balance)	The irreversibility or the exergy destroyed using entropy balance and Eq. (10) (the decrease of exergy principle)
I	Compressor	$\dot{m}_1 = \dot{m}_2 = \dot{m}_r$ (102)	$\dot{E}x_1 + \dot{W}_{comp,e} = \dot{E}x_{2a} + \dot{I}_I$ (103)	$\dot{I}_I = T_0 \dot{m}_r (s_1 - s_{2a})$ (105)
			$\dot{I}_I = \dot{m}_r(\psi_1 - \psi_{2a}) + \dot{W}_{comp}$ (104)	
II	Condenser	$\dot{m}_1 = \dot{m}_2 = \dot{m}_r$ (106)	$\dot{E}x_{2a} + \dot{E}x_6 = \dot{E}x_3 + \dot{E}x_5 + \dot{I}_{II}$ (108)	$\dot{I}_{II} = T_0[\dot{m}_r(s_3 - s_{2a}) + \dot{m}_w(s_5 - s_6)]$ (110)
		$\dot{m}_5 = \dot{m}_6 = \dot{m}_w$ (107)	$\dot{I}_{II} = \dot{m}_r(\psi_{2a} - \psi_3) + \dot{m}_w(\psi_6 - \psi_5)$ (109)	
III	Throttling valve (capillary tube)	$\dot{m}_3 = \dot{m}_4 = \dot{m}_r$ (111)	$\dot{E}x_3 = \dot{E}x_4 + \dot{I}_{III}$ (112)	$\dot{I}_{III} = T_0 \dot{m}_r (s_4 - s_3)$ (114)
			$\dot{I}_{III} = \dot{m}_r(\psi_3 - \psi_4)$ (113)	
IV	Evaporator	$\dot{m}_4 = \dot{m}_1 = \dot{m}_r$ (115)	$\dot{E}x_4 + \dot{E}x_8 = \dot{E}x_1 + \dot{E}x_7 + \dot{I}_{IV}$ (116)	$\dot{I}_{IV} = T_0[\dot{m}_r(s_1 - s_4) + \dot{m}_{wa}(s_7 - s_8)]$ (118)
			$\dot{I}_{IV} = \dot{m}_r(\psi_4 - \psi_1) + \dot{m}_{wa}(\psi_8 - \psi_7)$ (117)	
V	Fan coil units	$\dot{m}_{air,in} = \dot{m}_{air,out} = \dot{m}_{air}$ (119)	$\dot{E}x_5 = \dot{E}x_6 + \dot{Q}_{fc}\left(\frac{T_{in,air} - T_0}{T_{in,air}}\right) + \dot{I}_V$ (120)	$\dot{I}_V = T_0\left[\dot{m}_w(s_6 - s_5) + \frac{\dot{Q}_{fc}}{T_{in,air}}\right]$ (122)
			$\dot{I}_V = \dot{m}_w(\psi_5 - \psi_6) - \dot{Q}_{fc}\left(1 - \frac{T_0}{T_{in,air}}\right)$ (121)	
VI	Ground heat exchanger	$\dot{m}_7 = \dot{m}_8 = \dot{m}_{wa}$ (123)	$\dot{E}x_7 + \dot{Q}_{gh}\left(\frac{T_{soil} - T_0}{T_{soil}}\right) = \dot{E}x_8 + \dot{I}_{VI}$ (124)	$\dot{I}_{VI} = T_0\left[\dot{m}_{wa}(s_8 - s_7) - \frac{\dot{Q}_{gh}}{T_{soil}}\right]$ (126)
			$\dot{I}_{VI} = \dot{m}_{wa}(\psi_7 - \psi_8) + \dot{Q}_{gh}\left(1 - \frac{T_0}{T_{soil}}\right)$ (125)	

For further details, some relevant studies published should be taken into account [93–97].

Using Eq. (15), exergy efficiency relations for the GSHP unit and the whole system are written as follows:

$$\varepsilon_{\text{o,R,HP}} = \frac{\dot{\text{E}}\text{x}_{\text{heat}}}{\dot{W}_{\text{a,in}}} = \frac{\dot{\text{E}}\text{x}_{\text{cond,in}} - \dot{\text{E}}\text{x}_{\text{cond,out}}}{\dot{W}_{\text{a,in}}}, \tag{127}$$

$$\varepsilon_{\text{o,R,sys}} = \frac{\dot{\text{E}}\text{x}_{\text{heat}}}{\dot{W}_{\text{a,in}} + \dot{W}_{\text{pumps}} + \dot{W}_{\text{fan-coil}}}, \tag{128}$$

$$\varepsilon_{\text{HP}} = \frac{\text{COP}_{\text{a,h}}}{\text{COP}_{\text{C,h}}}, \tag{129}$$

$$\varepsilon_{\text{HP}} = \frac{\dot{P}_{\text{T,HP}}}{\dot{F}_{\text{T,HP}}}, \tag{130}$$

$$\varepsilon_{\text{sys}} = \frac{\dot{P}_{\text{T,sys}}}{\dot{F}_{\text{T,sys}}}. \tag{131}$$

Exergy analysis has been applied to various types of heat pumps by a number of researchers [i.e., 41,50,51,56,98–100]. However, the studies on exergy analysis of GSHPs are relatively few in numbers [93–97,101–103]. Some of them [i.e., 43,104] have been included in the exergoeconomic (a combination of exergy and economics) analysis of GSHP systems. The first detailed exergetic evaluation of a GSHP system was made by Hepbasli and Akdemir [95] to the current knowledge of the author, while Ozgener and Hepbasli [105] also conducted a comprehensive review on the energy and exergy analysis of solar assisted heat pump systems. In this regard, the performance of this GSHP system with a 50 m vertical 32 mm diameter U-bend ground heat exchanger was assessed using energy and exergy analysis methods. Fig. 22 [94] illustrates a graphical representation of the exergy balance, namely the Grassmann diagram, for the GSHP system. This diagram, on the other hand, gives quantitative information regarding the proportion of the exergy input to the system that is dissipated in each of the components. As can be seen in Fig. 22, the highest irreversibility occurred in sub-region I, the motor-compressor subassembly. The total magnitude of the losses was over 56% of the actual power input, while the mechanical–electrical losses accounted for 46% of that. These losses were due to the electrical, mechanical and isentropic efficiencies and emphasize the need for paying close attention to the selection of this type of equipment, since components of inferior performance could considerably reduce the overall performance of the system. The second largest irreversibility was due to the condenser. This was partly due to the large degree of superheat achieved at the end of the compression process, leading to large temperature differences associated with the initial phase of heat transfer. The third highest irreversibility was in the capillary tube due to the pressure drop of the refrigerant passing through it. Besides this, the evaporator had the lowest irreversibility on the basis of the heat pump cycle [95].

Table 8 [93–97,103,106,107] lists various ground source (geothermal) heat pumps analyzed using exergy analysis method Five types of exergy efficiencies given in Eqs. (127)–(131) were used in the calculations. It is obvious from this table that the

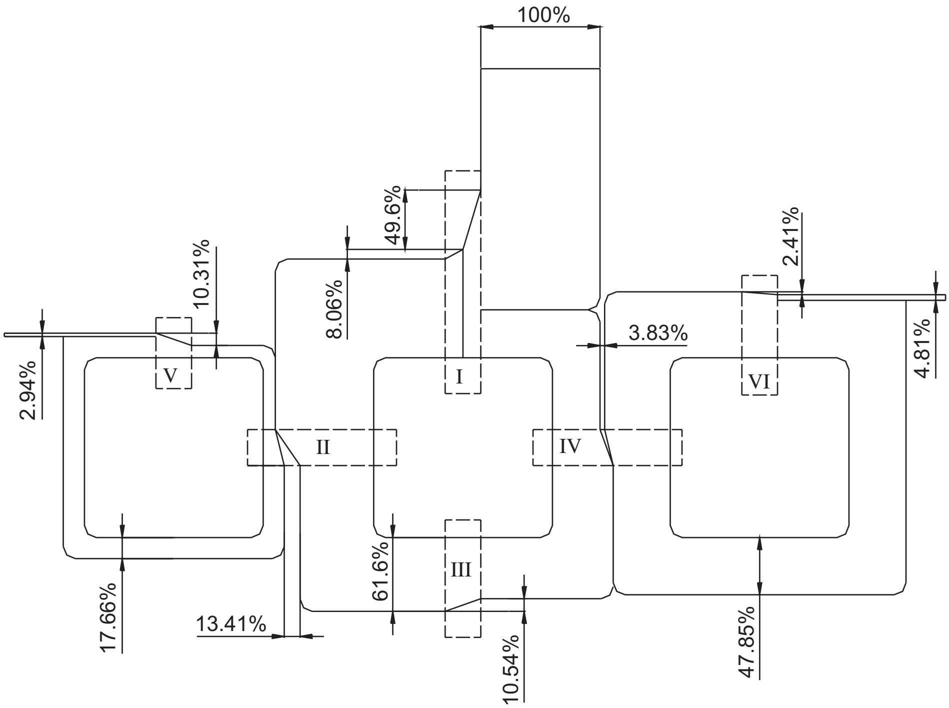


Fig. 22. Exergy diagram (the Grassmann diagram) for the GSHP system [94]. (I) Compressor, (II) condenser, (III) capillary tube, (IV) evaporator, (V) fan-coil units, (VI) ground heat exchanger.

exergy efficiency values of GSHP units vary between about 67% and 92% on the product/fuel basis depending on the various dead state temperatures. The values for the exergy improvement rate and thermodynamic parameters calculated using Eq. (16) and Eqs. (17)–(20) were also included in this table.

4.3.2.3. Greenhouses. Good plant-growth conditions can be achieved by using greenhouses. A greenhouse can be managed to protect the plants by creating a favorable environment, allowing intensive use of soil, and helping sanitary plant control. A variety of heating systems are being used in present day greenhouses to meet the heating and cooling requirements. As an alternative, there is great potential in employing a heat pump system for greenhouse air-conditioning based on its ability to perform the multi-function of heating, cooling and dehumidification [11].

Although various studies were undertaken to evaluate the performance of solar assisted heat pump systems, to the best of author's knowledge, two studies [11,14] have appeared in the open literature on the experimental performance testing of a solar assisted vertical GSHP system for greenhouse heating. The first one [11] was related to an exergetic assessment at a fixed dead state temperature, while the second one [14] included a parametric study investigating the effect of varying dead state temperature on the exergy efficiencies.

Table 8
Various ground source (geothermal) heat pumps analyzed using exergy analysis method [93–97,103,106,107]

Location of the system built/ country	Type of heat pump/ operating mode	Capacity in the mode operated (kW)	Dead state temp. (°C)	Date of data used	Exergy destructions (*rate of improvement potential*) (% of the whole heat pump system)								Eq. no. for exergy eff.	Exergy efficiency (%)		Thermodynamic parameters for compressor (% of the whole system)				Ref.
					Ground source heat pump system (Whole system)[a]															
					Ground source heat pump unit				Other components					Heat pump	Overall	χ	δ	ξ	f	
					I Com.	II Con.	III Thr. valve	IV Evap.	V Fan-coil/ Con. WT	VI GHE /PHEx	VII Cir. pumps	VIII Sol. col.								
Izmir/ Turkey	Vertical GSHP/heating (for space heating)	3.41	20	Feb. 2001	16.54	27.91	21.62	7.83	21.14				(127) (129)		2.94 3.84	51.8	23.6	35.4	40.2	[95]
Izmir/ Turkey	Vertical GSHP/heating (for space heating)	4.27	2.2	7 Jan.2004	51.83 *(57.12)*	8.00 *(3.03)*	8.36 *(2.43)*	9.42 *(14.30)*	17.67 *(17.21)*				(127) (128) (130) (131)	9.07 66.8 	 8.4 66.6					[93]
Izmir/ Turkey	Solar assisted vertical GSHP/ heating (for greenhouse heating)	3.98	10.93	17 Dec. 2003–17 March 2004	28.33	13.85	11.34	8.19	30.22	2.52	1.83 and 3.09	0.63	(130) (131)	71.8	 67.7	28.3	9.1	13.5	30.4	[94]
Izmir/ Turkey	Solar assisted vertical GSHP/ heating (for greenhouse heating)	4.15	−0.69	7 Jan. 2004	23.06	10.45	6.53	9.79	43.11	2.61	1.24 and 1.89	1.30	(130) (131)	76.2	 75.6	23.1	5.6	7.4	21.1	[96]

Table 8 (*continued*)

Location of the system built/country	Type of heat pump/operating mode	Capacity in the mode operated (kW)	Dead state temp. (°C)	Date of data used	Exergy destructions (*rate of improvement potential*) (% of the whole heat pump system)								Eq. no. for exergy eff.	Exergy efficiency (%)		Thermodynamic parameters for compressor (% of the whole system)				Ref.
					Ground source heat pump system (Whole system)[a]															
					Ground source heat pump unit				Other components					Heat pump	Overall	χ	δ	ξ	f	
					I Com.	II Con.	III Thr. valve	IV Evap.	V Fan-coil/Con. WT	VI GHE/PHEx	VII Cir. pumps	VIII Sol. col.								
Izmir/Turkey	Solar assisted vertical GSHP/heating (for greenhouse heating)	3.97	1.00	17 Dec. 2003–17 March 2004	3.13	17.70	13.68	6.43	49.08	8.61	0.8	0.57	(130) (131)	91.80	 86.13					[103]
Erzurum/Turkey	GSHP with water source/heating (for space heating)[b]	7.02	25		45.92	15.83	6.27	11.69	14.64	/5.66			(130) (131)	4.64	 1.44					[97]

[a]I-Com: compressor, II-Con: condenser, III-Thr. valve: throttle (expansion) valve, IV-Evap: evaporator, V: Fan-coil,/Con. WT: condenser water tank, VI-GHE: ground-heat exchanger/PHEx: plate heat exchanger, VII-Cir. Pumps: circulating pumps, VIII-Sol. col.: solar collector.

[b]This system was designed and constructed by Kara [106] in 1999 on the base of a PhD thesis in the Mechanical Engineering Department, Ataturk University, Erzurum in Turkey in order to evaluate geothermal resources with low temperatures. The performance of the system was evaluated by Kara and Yuksel [107] using the energy analysis method only, while this system was evaluated by Akpinar and Hepbasli [97] using exergy analysis method.

A schematic diagram of the constructed experimental system is illustrated in Fig. 23 [11,14]. This system mainly consists of three separate circuits as follows:(i) the ground coupling circuit with solar collector (brine circuit or water-antifreeze solution circuit), (ii) the refrigerant circuit (or a reversible vapor compression cycle) and (iii) the fan-coil circuit for greenhouse heating (water circuit).

The exergetic results of these two studies are illustrated in Table 8. The highest irreversibility on a system basis occurred in the greenhouse fan-coil unit, followed by the compressor, condenser, expansion valve and evaporator, sub-regions I and V for the GSHP unit and the whole system, respectively. Besides this, the remaining system components have a relatively low influence on the overall efficiency of the whole system. Experimental have also showed that monovalent central heating operation (independent of any other heating system) could not meet overall heat loss of greenhouse if ambient temperature was very low. The bivalent operation (combined with other heating system) could be suggested as the best solution in Mediterranean and Aegean regions of Turkey, if peak load heating could be easily controlled [11].

4.3.2.4. Drying. Large quantities of food products are dried to improve shelf life, reduce packing costs, lower shipping weights, enhance appearance, encapsulate original flavor and maintain nutritional value. In evaluating the performance of food systems, energy analysis method has been widely used, while studies on exergy analysis, especially on exergetic assessment of drying process, are relatively few in numbers [108–112]. In these previous studies, the drying process was thermodynamically modeled by Dincer and Sahin [109], while drying of different products such as pistachio [108], red pepper slices [110], potato [111], pumpkin [112], wheat kernel [113] and apple slices [114] was evaluated in terms of energetic and exergetic aspects using various drying devices, such as a fluidized bed dryer, a solar drying cabinet, and cyclone type dryers [115]. Based on the previous studies, the first study on exergetic evaluation of a drying process using a GSHP drying system appears to be done by Kuzgunkaya and Hepbasli [115], who used laurel leaves as a product being dried, and made a comparison of exergetic efficiency values obtained from various studies on food drying systems. The main objective of this contribution was to perform exergy analyses of the drying process in terms of drying of laurel leaves under different operating conditions for the assessment of the drying performance.

Fig. 24 [115] illustrates a schematic diagram of this system, which consists of mainly three separate circuits, namely: (I) the ground coupling circuit (brine circuit or water–antifreeze solution circuit), (II) the refrigerant circuit (or a reversible vapor compression cycle) and (III) the drying cabinet circuit (air circuit). The main components of the heat pump system are an evaporator, a condenser, a compressor and an expansion valve. To avoid freezing the water under the working condition and during the winter, a 10% ethyl glycol mixture by weight was prepared. The refrigerant circuit was built on the closed loop copper tubing. The working fluid was R-22 [115].

There are mainly two ways of formulating exergetic efficiency for drying systems [108,113,115]. The first one can be defined as the ratio of the product exergy to exergy inflow as follows [108,115]:

$$\eta_{ex} = \frac{\text{Exergy inflow} - \text{Exergy loss}}{\text{Exergy inflow}} = 1 - \frac{\dot{E}x_{loss}}{\dot{E}x_{in}}. \quad (132)$$

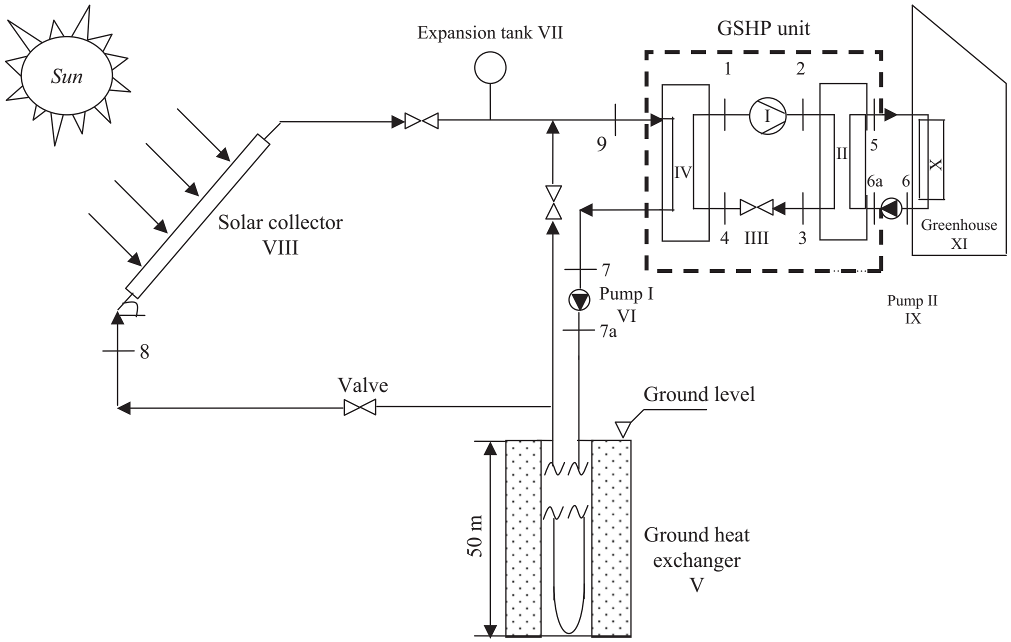


Fig. 23. A schematic diagram of a solar asissted vertical ground source heat pump system for greenhouse heating [11,14].

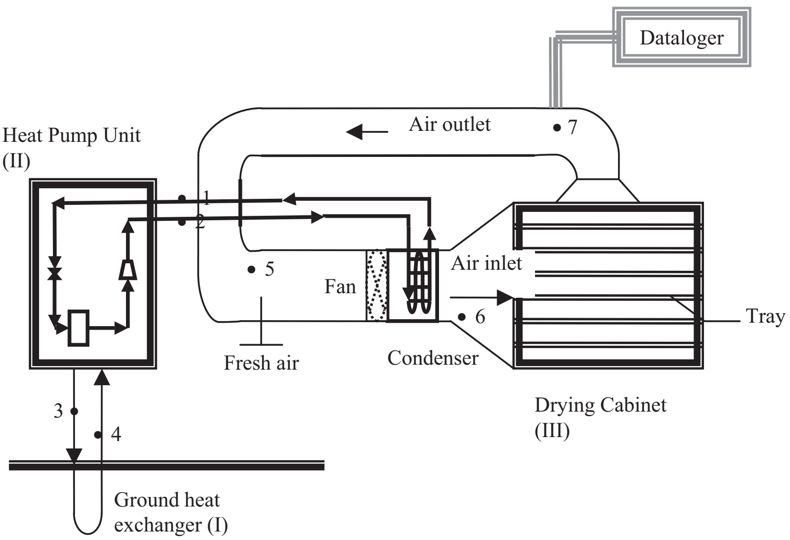


Fig. 24. Schematic diagram of the heat pump tray drying system [116]. (1) Refrigerant inlet to the expansion valve, (2) refrigerant outlet from the compressor, (3) water inlet to the ground heat exchanger, (4) water outlet from ground-heat exchanger, (5) air inlet to the condenser, (6) air outlet from the condenser, (7) air outlet from the drying chamber.

The second one may be defined on the product/fuel basis, as given in Eq. (133). The product is the rate of exergy evaporation ($\dot{E}x_{evap}$) and the fuel is the rate of exergy drying air entering the dryer chamber ($\dot{E}x_{da}$). In this regard, exergy efficiency may be written as follows [113].

$$\eta_{ex} = \frac{\dot{E}x_{evap}}{\dot{E}x_{da}} \tag{133}$$

with

$$\dot{E}x_{evap} = \left[\left(1 - \frac{T_0}{T_{m_2}}\right)\dot{Q}_{evap}\right] \tag{134}$$

and

$$\dot{Q}_{evap} = \dot{m}_w h_{fg}, \tag{135}$$

where $\dot{Q}_{evap}$ is the heat transfer rate due to phase change, T_{m_2} is the exit temperature of the material, $\dot{m}_w$ is the mass flow rate of water and h_{fg} is the vaporization latent heat.

The laurel leaves were sufficiently dried at the temperatures ranging from 40 to 50 °C with relative humidities varying from 16% to 19% and a drying air velocity of 0.5 m/s during the drying period of 9 h. The exergy efficiency values were obtained to range from 81.35% to 87.48% using Eq. (132) based on the inflow, outflow and loss of exergy, and 9.11% to 15.48% using Eq. (133) based on the product/fuel basis between the same drying air temperatures with a drying air mass flow rate of 0.12 kg/s [116].

A comparison of exergy efficiency values in drying various products is made in Table 9 [108,112,113,115]. It is obvious from this table that the exergy efficiency values calculated using Eq. (132) are quite higher than those using Eq. (133). It may be concluded that it is more meaningful, objective and useful to assess the performance of the drying process relative to the performance of similar drying processes on the product (or benefit)/fuel basis [116].

4.3.3. Indirect utilization (geothermal power plants)

Commercial delivery of geothermally generated electric power occurred in 1914 when a 250 kW unit at Larderello provided electricity to the nearby cities of Volterra and Pomarance [116]. Since then, many geothermal power plants have been installed. The performance of these systems has been mostly evaluated using energy analysis method, while the number of the geothermal plants, of which performance has been assessed using exergy analysis method, is very low. The concept of exergy was first used to analyze a geothermal power plant by Badvarsson and Eggers [117]. Their illustrative example, which compared the performances of single and double flash cycles based on a reservoir water temperature of 250 °C and a sink condition of 40 °C, gave exergetic efficiencies of 38.7% and 49%, respectively, assuming 65% mechanical efficiency [71].

Using Eq. (15) along with its concept and applying it to a power plant as a whole, the overall exergetic efficiency reduces to a very simple formula, namely, the ratio of the net power output ($\dot{W}_{net,plant}$) to the exergy of the motive fluid serving as the energy source for the plant [118]. That is:

$$\varepsilon_{g,pp} = \frac{\dot{W}_{net,plant}}{\dot{E}x_{wh}}, \tag{136}$$

Table 9
Comparison of exergy efficiency values calculated by some investigators in drying various products [108,112,113,115]

Investigators/year of publication	Type of dryer	Product dried			Air			Exergy efficiency	
		Type	Initial moisture content (%)	Final moisture content on dry weight basis (%)	Velocity (m/s)	Temperature (°C)	Relative humidity (%)	Eq. no.	Value (%)
Syahrul et al. [113]	Fluidized bed dryer	Red-spring wheat	31.7–32.6	15	1.95	40.2–65	18.5–21.1	(133)	4–12
		Corn	24.6–25.6		2.22–2.24	50–63	15.2–17.5		2–16
Midilli and Kucuk [108]	Solar drying cabinet	Shelled/ unshelled pistachios	26.95/29		1.23	40–60	37–62	(132)	10.86–100
Akpinar et. al. [112]	Cyclone type dryer	Pumpkin slices		6	1.5	60	10–20	(132)	30.81–100
				6		70			37.89–100
				4		80			46.97–100
Kuzgunkaya and Hepbasli [115]	Ground-source heat pump dryer	Laurel leaves	94.4	12	0.5	40	16–19	(132)	81.35–87.48
						50		(133)	9.11–15.48
						40			
						50			

$$\varepsilon_{g,pp} = \frac{\dot{W}_{net,plant}}{\dot{Ex}_{res}}, \tag{137}$$

where $\dot{Ex}_{wh}$ and $\dot{Ex}_{res}$ are the total exergy inputs to the plant at wellhead and reservoir conditions, respectively, while they are calculated using Eqs. (6c) and (7).

Note that the exergy input to the plant is sometimes taken as the exergy of geothermal fluid in the reservoir. Those who prefer this approach argue that a realistic and most meaningful comparison between geothermal power plants can only be performed considering the methods of harvesting the geothermal fluid. However, others argue that taking the reservoir as the starting point is not proper for geothermal power plants since conventional power plants are evaluated on the basis of the exergy of the fuel burned at the plant site [118,119].

Exergetic efficiencies of some geothermal power plants worldwide in order of increasing efficiency are summarized by the author, as illustrated in Table 10 [119,120–127]. It is obvious from this table that exergy efficiencies vary from 16.3% to 53.9% depending on the dead state temperature and the technology used.

DiPippo [120] obtained the following correlation for the exergetic efficiency as a function of the dead-state temperature using the Brady geothermal power plant:

$$\varepsilon_{Brady} = 23.177 - 0.1429T_0. \tag{138}$$

DiPippo [120] concluded as follows: "Geothermal binary plants are relatively poor converters of heat into work. Thermal efficiencies typically lie in the range of 8–12%. As a consequence, a 1–2% point improvement in power output translates into a gain of about 10–20% in efficiency. The results show that binary plants can operate with very high exergetic efficiencies even when the motive fluids are low-temperature and low-exergy. Exergetic efficiencies of 40% or greater have been achieved in certain plants with geofluids having specific exergies of 200 kJ/kg or lower. The main design feature leading to a high-exergy efficiency lies in the design of the heat exchangers to minimize the loss of exergy during heat transfer processes. Another important feature that can result in a high exergy efficiency is the availability of low-temperature cooling water that allows a once-through system for waste heat rejection."

In the following, the Grassmann diagram of a 12.4 MW existing binary geothermal power plant is presented as an illustrative example of geothermal power plants. Exergy analysis of this plant was performed by Kanoglu [119] using actual plant data to assess the plant performance and the Grassmann shown in Fig. 25 [119] was drawn. As seen in this figure, the causes of exergy destruction in the plant included the exergy of the working fluid lost in the condenser, the exergy of the brine reinjected, the turbine-pump losses, and the preheater–vaporizer losses. The exergy destruction at these sites accounted for 22.6%, 14.8%, 13.9%, and 13.0% of the total exergy input to the plant, respectively.

Dagdas et al. [127] proposed a new model in order to improve efficiency and augment power output of the single flash type geothermal power plant operating in Denizli-Kızıldere, Turkey. In this model, electric energy requirement of the region would be met and performance of the geothermal power plant would be up rated by building a gas turbine power plant near the existing plant. If the proposed combined cycle power plant (gas turbine integrated geothermal power plant) would be operated, power generated in the geothermal plant could increase 43.5%. Energy and exergy efficiencies of the plant would be increased from 4.56% to 6.5%, and from 19.78% to 28.4%, respectively.

Table 10
Geothermal power plant exergetic efficiencies (in order of increasing efficiency) [119,120–127]

Technology	Plant name	Location/country	Dead state temperature (°C)	Exergy efficiency[a] (%)	Sources
Binary	Brady bottoming (p.m. data)	Churchill County, NV/USA	16.8	16.3	DiPippo [120]
Binary	Brady bottoming (a.m. data)	Churchill County, NV/USA	30.1	17.9	DiPippo [120]
Binary: recuperated	Rotokawa	Rotokawa/New Zealand		18.7	DiPippo [120]
Single flash	Kizildere	Denizli/Turkey	16	19.78[a] 19.97[b]	Dagdas et al. [121,127]
Single flash	Kizildere	Denizli/Turkey	16	20.5	Ozturk et al. [122]
Single flash	Kizildere	Denizli/Turkey	15	20.8	Cerci [123]
Single flash	Kizildere	Denizli/Turkey	18	24.3[b] 27.2[c]	Yildirim and Gokcen [124]
Binary	Nigorikawa (Mori) pilot	Hakodate on Hokkaido/Japan	13	21.6	DiPippo [120]
Binary	Kalina KCS 34, Husavik	Husavik/ Iceland	5	23.1	DiPippo [120]
Single flash	Kakkonda	Japan		26.5	Setiawan [125], Yildirim and Gokcen [124]
Binary: simple	Rotokawa	Rotokawa/New Zealand		27.8	DiPippo [120]
Single flash	Otake	Japan		29.0	Setiawan [125], Yildirim and Gokcen [124]
Dual-level binary		Northern NV/USA	12.8	29.1[d] 34.2[e]	Kanoglu [119]
Single flash	Salak (Unit 1&2)	Indonesia		30.4	Setiawan [125], Yildirim and Gokcen [124]

Binary: simple[f]	Kavala	Eratino/Greece	20	33.3[g] 8.1[g] 52.2[h]	Koroneos et al. [126]
Single flash	Ahuachapan (Unit 1 & 2)	El Salvador		33.1	Setiawan [125], Yildirim and Gokcen [124]
Single and double flash	Cerro-Prieto	Mexico		33.2	Setiawan [125], Yildirim and Gokcen [124]
Single and double flash	Ahuachapan (Unit 1 & 2)	El Salvador		38.2	Setiawan [125], Yildirim and Gokcen [124]
Single flash	Blundell	Near Milford in Beaver County/USA		35.6	DiPippo [120]
Hybrid flash-binary	Rotokawa	Rotokawa/New Zealand		42.0	DiPippo [120]
Binary: dual-level	Heber SIGC	Imperial Valley, CA/USA	15	43.4	DiPippo [120]
Double flash	Beowawe	NV/USA		46.0	DiPippo [120]
Dry steam	Kamojang (Unit 2 & 3)	Indonesia		48.4	Setiawan [125], Yildirim and Gokcen [124]
Dry steam	Darajat	Indonesia		52.4	Setiawan [125], Yildirim and Gokcen [124]
Binary: flash evaporator	Otake pilot	Island of Kyushu/Japan	18	53.9	DiPippo [120]

[a]Exergy efficiencies except those denoted in the above table are based on reservoir exergy.
[b]At reservoir conditions.
[c]At wellhead conditions.
[d]Based on the exergy of the geothermal fluid at the vaporizer inlet.
[e]Based on the exergy drop of the brine across the vaporizer-preheater system (i.e., exergy input to the Rankine cycle).
[f]For the exploitation of the field, a Rankine cycle is proposed by Koroneos et al. [126].
[g]For the first deposit based on the two case studies.
[h]For the second deposit.

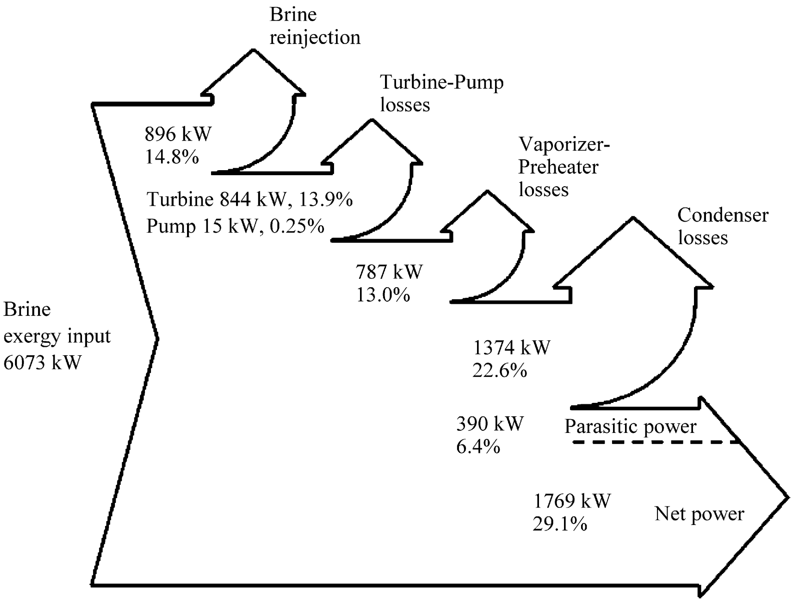


Fig. 25. Grassmann (exergy flow) diagram of a 12.4 MW existing binary geothermal power plant drawn by Kanoglu [119].

4.4. Biomass

Chemical exergy of a substance is the maximal possible useful work that may be produced by process of physical and chemical equilibration of the substance with the ambient. To evaluate the chemical exergy of a mixture, the knowledge of its enthalpy of combustion, elemental composition and absolute entropy is necessary. When some of these data are absent, the methods of estimation of energy are used [128]. The chemical exergy of gaseous and some liquids can be obtained using standard chemical exergy tables given in Ref. [7] if the chemical composition of the fuel is known. Many technical liquid and solid fuels are multi-component solutions (or mixtures) of very complicated, usually unknown components. An exact solution of the chemical exergy of such fuels is impossible. In this regard, Rant's relation including a constant ratio of chemical exergy and calorific value (or heating value) for liquid and (separately) for solid fuels ($\dot{E}x_{CH}/HV$) may be used. However, the calculation for different organic substances indicated that the ratio ($\dot{E}x_{CH}/HV$) depends significantly on the chemical composition.

If the elemental composition is known, the chemical exergy of various fuels can be evaluated accurately using the Szargut's correlations listed elsewhere [7]. In addition, a correlation formula to estimate chemical exergies of oil fractions and fuel mixtures from enthalpy of combustion and atomic composition developed by Govin et al. [128] is used.

Based approximation method for fuel chemical exergy (ψ_{ch}), the following relations are widely used.

$$\beta_{LHV} = \frac{\dot{E}x_{CH}}{LHV}, \tag{139}$$

$$\beta_{\text{HHV}} = \frac{\dot{\text{E}}\text{x}_{\text{CH}}}{\text{HHV}}, \tag{140}$$

where β is the proportionality constant (or quality factor or exergy coefficient), while LHV and HHV denote the lower heating (net caloric) and higher heating (gross caloric) values, respectively [129].

Szargut [22] proposed that β_{LHV} and β_{HHV} may be taken to be approximately 1.15 and 1.05 for wood, respectively. The following relations for wood with the limit of $(Z_{O_2}/Z_C) \leqslant 2.67$ are proposed by Szargut et al. [7] and Szargut [22], respectively.

$$\begin{aligned}\beta_{\text{LHV}} = \{&1.0412 + 0.2160(Z_{H_2}/Z_C) - 0.2499(Z_{O_2}/Z_C)[1 + 0.7884(Z_{H_2}/Z_C)] \\ &+0.0450(Z_{N_2}/Z_C)\}/\{1 - 0.3035(Z_{O_2}/Z_C)\}\end{aligned} \tag{141}$$

and

$$\begin{aligned}\beta_{\text{LHV}} = \{&1.0412 + 0.2160(Z_{H_2}/Z_C) + 0.2499(Z_{O_2}/Z_C)[1 + 0.7884(Z_{H_2}/Z_C)] \\ &+0.0450(Z_{N_2}/Z_C)\}/\{1 + 0.3035(Z_{O_2}/Z_C)\},\end{aligned} \tag{142}$$

where Z_i is mass fraction of element i.

Eq. (141) has been successfully used by some investigators [130–132]. In this regard, Nilsson [130] used the following relation for determining the specific chemical exergy of straw

$$\text{Ex}_{\text{CH,straw}} = (\text{LHV} + L_{\text{w}}Z_{\text{w}})\beta_{\text{LHV}} + \text{Ex}_{\text{CH,w}}Z_{\text{w}}, \tag{143}$$

where L and Z denote the enthalpy of phase change (kJ/kg) and the mass fractions (—), respectively. Using the following data for moist straw; $Z_C = 38.9\%$, $Z_{H_2} = 4.9\%$, $Z_{O_2} = 33.8\%$, $Z_{N_2} = 0.4\%$, $Z_w = 18.0\%$, $\text{LHV} = 13{,}800\,\text{kJ/kg}$, $L_w = 2440\,\text{kJ/kg}$ and $\text{Ex}_{\text{CH,w}} = 50\,\text{kJ/kg}$, the specific chemical exergy was calculated to be 16,100 kJ kg. In other words, the ratio of chemical exergy to the lower heating value was 1.16. In the calculation, the reference temperature was 25 °C, the relative humidity of atmospheric air was 70% and the chemical exergy of ash was neglected.

Panopoulos et al. [132] analyzed exergetically the combination of allothermal biomass gasification and solid oxide fuel cell for small scale CHP, and presented exergy efficiency relations. They also determined that for SOFC operation at current density 2500 A/m^2, the system used 90 kg/h biomass and operated with electrical exergetic efficiency 32% producing 140 kW$_e$, while the combined electrical and thermal exergetic efficiency was 35%.

Franco and Giannini [133] analyzed the perspective of improving the efficiency of biomass for power generation and proposed an exergy loss based economic analysis of biomass utilization. A thermoeconomic method of analysis based on the consideration of the cost of the exergy losses showed how the conversion efficiency of renewable sources as biomass, had a lower limit that, in a lot of cases, was considerably higher than the actual efficiency level.

According to Shieh and Fan [134], specific chemical exergy (kJ/kg) of structurally complicated materials, e.g. biomass, can be estimated from their elemental compositions as given below [135]

$$\begin{aligned}\psi_{\text{CH}} = 4.1868\{&8177.79[\text{C}] + 5.25[\text{N}] + 27,892.63[\text{H}] - 3173.66[\text{O}] \\ &+ 0.15[\text{O}](7837.677[\text{C}] + 33,888.889[\text{H}] - 4236.1[\text{O}]\}.\end{aligned} \tag{144}$$

Table 11
The calculated exergy values of various of woody biomass types in Turkey [136]

Type of wood	Ultimate analysis (%)				Exergy (MJ/kg)	HHV (MJ/kg)	β_{HHV}
	C	H	O	N			
Hus wood	48.5	5.6	45.7	0.2	17.90	17.22	1.040
Willow wood	50.8	6.0	42.5	0.6	19.63	19.01	1.033
Sugar cane	47.3	6.2	46.2	0.3	18.15	17.52	1.036
Olive residue	49.5	6.3	43.7	0.5	19.39	18.77	1.033
Straw	47.0	6.1	46.4	0.5	17.90	17.25	1.038
Corn cob	46.2	6.3	47.2	0.3	17.75	17.12	1.037
Olive shell	52.4	6.0	40.4	1.5	20.45	19.76	1.031
Wheat straw	48.7	6.2	44.8	0.3	18.83	18.21	1.034
Rice shall	48.7	6.0	44.7	0.6	18.60	17.96	1.036
Rice straw	47.0	6.4	45.5	1.1	18.38	17.77	1.034
Hybride poplar	51.6	6.3	41.5	0.6	20.42	19.84	1.029
Cotton stalk	46.7	6.2	46.5	0.6	17.90	17.96	1.037

Bilgen et al. [136] studied on exergy analyses of various types of wood and coal samples with Turkish origins by using exergy analysis method developed and published by Srivastava [137] and Bejan et al. [138]. They calculated the exergy values of various of woody biomass types in Turkey, as given in Table 11 [136]. As can be seen in this table, the values for β_{HHV} vary from 1.029 to 1.040. On the other hand, these values were found greater than 1.0 for all the woody biomass types. Bilgen et al. [136] concluded that this result proposed that maximum work is always greater than the heating value, or energy delivered by a process in which these coals are used as a functional material.

Utlu et al. [139] evaluated the Turkish cotton stalk production in 2003 using energy and exergy analysis method for the first time. The values for the net energy and exergy gained were obtained to be about 49,146 and 38,426 MJ/ha, respectively. The overall mean energy and exergy efficiencies of the cotton production in the year studied were found to be 33.06% and 33.12%, respectively.

Prins et al. [140] performed laboratory experiments in a small-scale (5–10 g sample) fixed-bed torrefaction reactor placed inside an oven and gave exergetic efficiency relations for various processes. They reported as follows: Overall exergetic efficiency of air-blown gasification of torrefied wood was lower than that of wood since the volatiles produced in the torrefaction step were not utilized. For the entrained flow gasifier, the volatiles could be introduced into the hot product gas stream as a 'chemical quench'. The overall efficiency of such a process scheme was comparable to direct gasification of wood, but more exergy was conserved in as chemical exergy in the product gas (72.6% versus 68.6%).

4.5. Other renewable energy systems

The following section summarizes exergy relations for ocean surface waves, precipitation, ocean thermal gradient and tides, which have been taken from a study conducted by Hermann [14]. These relations may be used in exergetic evaluating these types of RERs.

4.5.1. Ocean surface waves

The average specific exergy of surface waves ranges from 10 to 100 kW/m, with much higher values during storms [14,141]. The waves concentrate kinetic energy transfer from the wind over many kilometers and can deposit this energy at the coastline. The primary factors determining the exergy of a fluid gravity wave are the period and [14,142]. For an approximately sinusoidal deep ocean wave, the length-specific exergy flux is

$$\psi_{\text{wave}} = \frac{1}{2}\rho V_{\text{wave}} g a_{\text{wave}}^2, \tag{145}$$

where V_{wave} is the wave speed, g is the gravitational constant and a_{wave} is the amplitude.

4.5.2. Precipitation

The specific exergy of precipitation can be broken down into physical and chemical components due to its gravitational and diffusive chemical potential energy relative to seawater.

For a specific replenishing body of water such as a dammed reservoir, the gravitational potential exergy is

$$\psi_{\text{pre,pot}} = \dot{m} g z, \tag{146}$$

where $\dot{m}$ is the mass flow rate and z is the vertical distance from the water level of the reservoir to the reference height or average sea level [14].

Precipitation also contains a diffusive exergy component due to the difference in chemical potential between the Earth's freshwater and seawater. Since the difference between seawater and freshwater is primarily dissolved salts, this value can be computed most directly by considering a reversible osmosis process.

The work done against the osmotic pressure is

$$\psi_{\text{pre,diff}} = -RT \ln(1 - y_{\text{solute}}), \tag{147}$$

where y is the mole fraction of solute in the water [14,143].

4.5.3. Ocean thermal gradient

The solar warming of seawater in the tropics and the radiative loss of thermal energy to space near the poles creates a density-driven current which circulates seawater from the surface to the deep ocean. Due to the small temperature differential, the exergy density of the ocean thermal gradient is relatively small. For a temperature difference of 20 K, the exergy content is approximately 7% of the thermal energy [14].

$$\psi_{\text{TEG}} = \dot{m} C_{\text{p,ave}}(T_{\text{warm}} - T_{\text{cold}})\left(1 - \frac{T_{\text{cold}}}{T_{\text{warm}}}\right). \tag{148}$$

4.5.4. Tides

The specific tidal exergy of a designated area of ocean or enclosed reservoir is a function of the record of minima and maxima and the time periods between these levels [14]. As the tide rises and falls, an average exergy flow considering the reservoir area integrated over the height difference between local maxima and minima and the period between these points can be written as follows:

$$\psi_{\text{tidal}} = \frac{1}{n}\sum_{n} \frac{\rho g \int_{z_{n-1}}^{z_n} A_{\text{res}}(z)\,\mathrm{d}z}{t_n}, \tag{149}$$

where t is the period between local maxima and minima of the tidal record, A_{res} the area of the reservoir at height z, and n the index number for each maximum or minimum [14].

4.6. Country based renewable energy sources

The method of exergy analysis has been applied to a wide variety of thermal and thermo chemical systems. A particular thermo dynamical system is the society, for example, of a country or a region [144]. In order to attain energy saving, the application of energy and exergy analysis modeling techniques for energy-utilization assessments has recently significantly increased. Utlu and Hepbasli [145] conducted a comprehensive review on the exergetic assessment of countries. In this regard, the approaches used to analyze energy utilization of countries or societies may be grouped into three types, namely Reistad's approach, Wall's approach and Sciubba's approach. In Reistad's approach, the end use is divided into three sectors, these names are industry, transportation and residential–commercial. In addition, energy sector with electric generation and distribution, oil refining, is treated separately. Flows of energy carriers for energy uses are not included in this approach. In Wall's approach, all types of energy and material flows are considered. However, to energy carriers for energy use are considered, these flows encompass wood for construction materials and for the pulp and paper industry, harvested wood and fodder, and the products from these materials. The so-called Sciubba's approach is relatively a new one. Extended-exergy accounting (EEA) method introduced by Sciubba was applied to the Italian society in 1996 by Milia and Sciubba [146] and recently to Norway with the figures of 2000 by Ertesvåg [147].

Table 12 [145,149,150] illustrates Eqs. (150)–(158) used to estimate exergy (second law) utilization efficiencies for the RERs. The exergy efficiency frequently gives a finer understanding of performance than (η). The parameter (ε) weights energy flows by accounting for each in terms of availability. It stresses that both losses and internal irreversibilities need to be dealt with to improve performance.

To date, various studies, as reviewed in detail elsewhere [145], were performed to analyze energy and exergy utilization efficiencies of countries in the four subsectors, namely utility, industrial, residential- commercial and transportation sectors. However, studies conducted on the evaluation of energy utilization efficiency of RERs using energy and exergy analyses are very limited in numbers in the open literature. The works done by Hepbasli and Utlu [15,148] on Turkey's RERs for the years of 2001 and 2010 appear to be the first ones.

Table 13 [15,148,151–154] illustrates the main outcomes of the exergy utilization analysis for both Turkey's general and RERs. It is clear from this table that the exergy utilization efficiencies for Turkey's general ranged from 13.10 to 27.94%. For Turkey's RERs, exergy utilization efficiencies varied from 24.14 and 44.30% in 2001 and 2010, respectively [15]. These results have clearly indicated the necessity of the planned studies towards increasing exergy utilization efficiencies in the sector studied. Hepbasli and Utlu [15] concluded that the analyses reported here would provide the investigators with knowledge about how much effective and efficient a country uses its natural resources, while this knowledge is also needed for identifying energy efficiency and/or energy conservation opportunities as well as for dictating the energy strategies of a country or a society, especially for a sustainable future.

Table 12
Relations used in the exergy analysis [145,149,150]

	Equations		Description
1	$\varepsilon = (\text{exergy in products}/\text{total exergy input}) \times 100$	(150)	Definition of exergy utilization efficiencies
2	$\varepsilon = (\eta/\beta)\{1 - [T_0/(T - T_0)]\ln(T/T_0)\}$	(151)	Exergy utilization efficiencies of space heating
3	$\varepsilon = (W_{out}/W_{in})100$	(152)	Exergy utilization efficiencies of RERs for utility sector
4	$\varepsilon = \eta[1 - (T_0/T)]$	(153)	Exergy utilization efficiencies of cooking
5	$\varepsilon = \eta[(T_0/T) - 1]$	(154)	Exergy utilization efficiencies of refrigeration
6	$\varepsilon_{oe} = [(a_1\varepsilon_{a1}) + (a_2\varepsilon_{a2}) + (a_3\varepsilon_{a3}) + \cdots + (a_7\varepsilon_{a7})]/100$	(155)	Overall sector exergy utilization efficiencies for electric use
7	$\varepsilon_{of} = [(f_{sh} \times \varepsilon_{sh,f}) + (f_{wh} \times \varepsilon_{wh,f}) + (f_c \times \varepsilon_{c,f})]/100$	(156)	Overall sector exergy utilization efficiencies for fuel use
8	$\varepsilon_{or} = [(r_{sh} \times \varepsilon_{2sh,or}) + (r_{wh} \times \varepsilon_{wh,orf}) + (r_c \times \varepsilon_{2c,ro})]/(r_{sh} + r_{wh} + r_c)$	(157)	Overall sector exergy utilization efficiencies for RE use
9	$\varepsilon_o = (\varepsilon_e e_{rc} + \varepsilon_{of} f_{exrc} + \varepsilon_r e_{exrc})/(e_{rc} + f_{exrc} + e_{exrc})$	(158)	Overall sector exergy utilization efficiencies for residential-commercial sector

Table 13
Comparison of total exergy inputs/outputs as well as exergy utilization efficiencies of Turkey's renewables and total [15,148,151–154]

Investigators	Year analyzed/published	Population	Total exergy input		Total exergy output		RERs[c] input[a]		RERs[c] output		Efficiencies	
			(PJ)	(GJ/cap)	(PJ)	(GJ/cap)	(PJ)	(GJ/cap)	(PJ)	(GJ/cap)	Total ε (%)	RERs[c] ε (%)
Unal [151]	1991/1994	57,024,515	2279	39.97	539.5	9.46	450.54	7.90			23.7	
Rosen and Dincer [152]	1993/1997	58,808,625	680.6	11.57	445.2	7.57	455.1	7.74			27.1	
Ileri and Gurer [153]	1995/1998	59,706,545	2697.3	45.17	352.3	5.9	474.4	7.95			13.1[b]	
Utlu and Hepbasli [154]	1999/	66,022,636	3380.34	51.2	499.61	7.55	459.25	6.96			24.04	
	2000/	67,803,927	3469.62	52.55	525.77	7.96	449.72	6.63			24.78	
Hepbasli and Utlu [15]	2001/2004	68,820,985	3139.07	45.61	783.75	11.39	395.68	5.75	95.51	1.38	25.22	24.14
Hepbasli and Utlu [148]	2010/	76,840,418	7400.34	96.31	2067.65	26.91	580.21	7.55	351.7	4.58	27.94	44.30

[a]These values are found by calculation from references.
[b]Excluding utility sector use. These values are obtained to be 43.61 (21.83)% with the utility sector use of 236.6 PJ.
[c]Renewable energy resources.

5. Conclusions

Exergetic aspects of RERs are comprehensively presented in this study. These RERs studied are solar, wind and geothermal energy systems as well as biomass and country based RERs. Studies conducted on these RERs are also compared with the previously ones in tabulated forms.

Some concluding remarks which can be extracted from this study are as follows:

(a) Exergy is a way to a sustainable development. In this regard, exergy analysis is a very useful tool, which can be successfully used in the performance evaluation of RERs as well as all energy-related systems.

(b) Based on the review results of the RERs, the following exergy efficiency values were found.

- The exergy efficiency of a SPC was found to range from 0.4% to 1.25% [33].
- The exergy efficiencies of a solar collector, a PV and a hybrid solar collector were found to be 4.4%, 11.2% and 13.3%, respectively. Solar collector had the lowest value. In terms of energy quality, the hybrid solar collector was very effective [67].
- Based on an exergetic evaluation of wind energy systems, average differences between energy and exergy efficiencies were obtained to be approximately 40% at low wind speeds and up to approximately 55% at high wind speeds [68].
- Geothermal resources should be classified by their exergy, a measure of their ability to do work. The classification with reference to SExI was more meaningful as there was no general agreement on the arbitrary temperature ranges used in the classification of geothermal resources by temperature [70,71].
- Based on a comparison of exergy efficiency values for GDHSs installed in Turkey, exergy efficiencies ranged from 42.94% to 66.13% depending on the various dead state temperatures. As expected, the lower the reference state temperature, the significantly larger the exergy losses in the system pipeline and heat exchangers [81–83,86,87,90,91].
- Exergy efficiency values of GSHP units varied between about 67% and 92% on the product/fuel basis depending on the various dead state temperatures [93–97,103,106,107].
- It was found from an exergetic evaluation of a drying process utilizing a GSHP system that the exergy efficiency values of the drying process ranged from 81.35% to 87.48% based on the inflow, outflow and loss of exergy, and 9.11% to 15.48% based on the product/fuel basis between the same drying air temperatures with a drying air mass flow rate of 0.12 kg/s. It was also concluded that it was more meaningful, objective and useful to assess the performance of the drying process relative to the performance of similar drying processes on the product (or benefit)/fuel basis [115].
- Exergetic efficiencies of some geothermal power plants worldwide were compared with each other and found to vary from 16.3% to 53.9% depending on the dead state temperature and the technology used [119,120,122–127].
- Exergy utilization efficiencies of Turkey's RERs were found to range from 24.14% and 44.30% in 2001 and 2010, respectively [15]. These results have clearly indicated the necessity of the planned studies towards increasing exergy utilization efficiencies in the sector studied.

(c) As a conclusion, the author expects that the analyses reported here will provide the investigators with knowledge about how effective and efficient a country uses its RESs. This very useful knowledge is also needed for identifying energy efficiency and/or energy conservation opportunities, as well as for dictating the right energy and exergy management strategies of a country.

Acknowledgement

The author is grateful for the support provided for the present work by Ege University, Izmir, Turkey. He also would like to express his appreciation to his wife Fevziye Hepbasli and his daughter Nesrin Hepbasli for their continued patience, understanding and full support throughout the preparation of this paper as well as all the other ones. The continuous incentive support given by the Scientific & Technological Research Council of Turkey (TUBITAK) is also gratefully acknowledged, while the author is grateful to Prof. Dr. Ibrahim Dincer, presently working at University of Ontario Institute of Technology (UOIT) in Canada, due to his continued support.

References

[1] Kaya D. Renewable energy policies in Turkey. Renew Sustain Energy Rev 2006;10:152–63.
[2] Boyle G, editor. Renewable energy: power for a sustainable future. Oxford: Oxford University Press; 1998. p. 1–40.
[3] Beccali M, Cellura M, Mistretta M. Environmental effects of energy policy in Sicily: the role of renewable energy. Renew Sustain Energy Rev 2007;11(2):282–98.
[4] Mígueza JL, López-Gonzálezb LM, Salac JM, Porteiroa J, Granadaa E, Moràna JC, et al. Review of compliance with EU-2010 targets on renewable energy in Galicia (Spain). Renew Sustain Energy Rev 2006;10:225–47.
[5] Dincer I. The role of exergy in energy policy making. Energy Policy 2002;30:137–49.
[6] Alqnne K, Saari A. Distributed energy generation and sustainable development. Renew Sustain Energy Rev 2006;10(6):539–58.
[7] Szargut J, Morris DR, Stewart FR. Exergy analysis of thermal, chemical, and metallurgical processes. USA: Edwards Brothers Inc.; 1998.
[8] Rosen MA, Dincer I. Exergy methods for assessing and comparing thermal storage systems. Int J Energy Res 2003;27(4):415–30.
[9] Rosen MA, Dincer I. Exergy-cost-energy-mass analysis of thermal systems and processes. Energy Conversi Manage 2003;4(10):1633–51.
[10] Rosen MA, Le MN, Dincer I. Efficiency analysis of a cogeneration and district energy system. Appl Therm Eng 2005;25(1):147–59.
[11] Koroneos C, Spachos T, Moussiopoulos N. Exergy analysis of renewable energy sources. Renew Energy 2003;28:295–310.
[12] Singh N, Kayshik SC, Misra RD. Exergetic analysis of a solar thermal power system. Renew Energy 2000;19(1&2):135–43.
[13] Bettagli N, Bidini G. Larderello-Farinello-Valle Secolo Geothermal Area: exergy analysis of the transportation network and of the electric power plants. Geothermics 1996;25(1):3–16.
[14] Hermann WA. Quantifying global exergy resources. Energy 2006;31(12):1685–702.
[15] Hepbasli A, Utlu Z. Evaluating the energy utilization efficiency of Turkey's renewable energy sources during 2001. Renew Sustain Energy Rev 2004;8:237–55.
[16] Dincer I, Hussain MM, Al-Zaharnah I. Energy and exergy use in public and private sector of Saudi Arabia. Energy Policy 2004;32(141):1615–24.
[17] Kilkis IB. Utilization of wind energy in space heating and cooling with hybrid. Energy Buildings 1999;30:147–53.

[18] Moran MJ. Availability analysis: a guide to efficiency energy use. Englewood Cliffs, NJ: Prentice-Hall; 1982.

[19] Balkan F, Colak N, Hepbasli A. Performance evaluation of a triple effect evaporator with forward feed using exergy analysis. Int J Energy Res 2005;29:455–70.

[20] Cornelissen RL. Thermodynamics and sustainable development: the use of exergy analysis and the reduction of irreversibility. PhD thesis, University of Twente, The Netherlands; 1997.

[21] Wall G. Exergy tools. Proc Inst Mech Eng 2003:125–36.

[22] Szargut J. Exergy method: technical and ecological applications. Southampton, Boston: WIT Press; 2005.

[23] Wepfer WJ, Gaggioli RA, Obert EF. Proper evaluation of available energy for HVAC. ASHRAE Trans 1979;85(1):214–30.

[24] Kotas TJ. The exergy method of thermal power plants. Malabar, FL: Krieger Publishing Company; 1995.

[25] DiPippo R. Second Law assessment of binary plants generating power from low-temperature geothermal fluids. Geothermics 2004;33:565–86.

[26] Van Gool W. Energy policy: fairly tales and factualities. In: Soares ODD, Martins da Cruz A, Costa Pereira G, Soares IMRT, Reis AJPS, editors. Innovation and technology-strategies and policies. Dordrecht: Kluwer; 1997. p. 93–105.

[27] Xiang JY, Cali M, Santarelli M. Calculation for physical and chemical exergy of flows in systems elaborating mixed-phase flows and a case study in an IRSOFC plant. Int J Energy Res 2004;28:101–15.

[28] Bejan A. Advanced engineering thermodynamics. New York: Wiley; 1988.

[29] Petela R. Exergy of undiluted thermal radiation. Sol Energy 2003;74:469–88.

[30] Candau Y. On the exergy of radiation. Sol Energy 2003;75:241–7.

[31] Petela R. Energy of heat radiation. J Heat Transfer 1964;86:187–92.

[32] Petela R. Exergy analysis of the solar cylindrical-parabolic cooker. Sol Energy 2005;79:221–33.

[33] Ozturk HH. Experimental determination of energy and exergy efficiency of the solar parabolic-cooker. Sol energy 2004;77:67–71.

[34] Szargut JT. Anthropogenic and natural exergy losses (exergy balance of the Earth's surface and atmosphere). Energy 2003;28:1047–54.

[35] Millan MI, Hernandez F, Martin E. Letter to the Editor. Comments on "Available solar energy in an absorption cooling process". Sol Energy 1997;61(1):61–4.

[36] Landsberg PT, Mallinson JR. Thermodynamic constraints. Effective temperatures and solar cells. Toulouse: CNES; 1976 (p. 27–46).

[37] Press WH. Theoretical maximum for energy from direct and diffuse sunlight. Nature 1976;264:734–5.

[38] Spanner DC. Introduction to thermodynamics. London: Academic Press; 1964.

[39] Badescu V. Maximum conversion efficiency for the utilization of multiply scattered solar radiation. J Phys D 1991;24:1882–5.

[40] Jeter SM. Maximum conversion efficiency for the utilization of direct solar radiation. Sol Energy 1981;26(3):231–6.

[41] Chaturvedi SK, Chen IDT, Kheireddine A. Thermal performance of a variable capacity direct expansion solar-assisted heat pump. Energy Convers Manage 1998;39(3/4):181–91.

[42] Eskin N. Performance analysis of a solar process heat system. Energy Convers Manage 2000;41:1141–54.

[43] Ucar A, Inalli M. Exergoeconomic analysis and optimization of a solar-assisted heating system for residential buildings. Build Environ 2006;41:1551–6.

[44] Svirezhev YM, Steinborn WH, Pomaz VL. Exergy of solar radiation: global scale. Ecol Model 2003; 169:339–46.

[45] Onyegegbu SO, Morhenne J. Transient multidimensional second law analysis of solar collectors subjected to time-varying insolation with difuse components. Sol Energy 1993;50(1):85.

[46] Eskin N. Transient performance analysis of cylindrical parabolic oncentrating collectors and comparison with experimental results. Energy Convers Manage 1999;40:175–91.

[47] Landsberg PT, Tonge G. Thermodynamics of the conversion of diluted radiation. J Phys A: Math Gen 1979;12:551.

[48] Xiaowu W, Ben H. Exergy analysis of domestic-scale solar water heaters. Renew Sustain Energy Rev 2005;9:638–45.

[49] Kalogirou SA. Solar thermal collectors and applications. Progr Energy Combust Sci 2004;30:231–95.

[50] Tsaros TL, Gaggioli RA, Domanski PA. Exergy analysis of heat pumps. ASHRAE Trans 1781–91.

[51] Bilgen E, Takahashi H. Exergy analysis and experimental study of heat pump systems. Exergy Int J 2002;2(4):259–65.

[52] Aprea C, Mastrullo R, Renno C. An analysis of the performances of a vapour compression plant working both as a water chiller and a heat pump using R22 and R417A. Appl Therm Eng 2004;24(4):487–99.
[53] Ma G, Li X. Exergetic behaviour for an air-source heat pump system with economizer coupled with scroll compressor. In: CD-Proceedings of the international green energy conference, Waterloo, Ontario, Canada, Paper No. IGEC-1-132, 12–16 June 2005.
[54] Ding Y, Chai Q, Ma G, Jiang Y. Experimental study of an improved air source heat pump. Energy Convers Manage 2004;45:2393–403.
[55] Badescu V. First and second law analysis of a solar assisted heat pump based heating system. Energy Convers Manage 2002;43:2539–52.
[56] Cervantes JG, Torres-Reyes E. Experiments on a solar-assisted heat pump and an exergy analysis of the system. Appl Therm Eng 2002;22(12):1289–97.
[57] Torres-Reyes E, Picon-Nunez M, Gortari C. Exergy analysis and optimization of a solar-assisted heat pump. Energy 1998;23(4):337–44.
[58] Pridasawas W, Lundqvist P. An exergy analysis of a solar-driven ejector refrigeration system. Sol Energy 2004;76:369–79.
[59] De Vos A. Endoreversible thermodynamics of solar energy. USA: Oxford University Press; 1992.
[60] Sozen A, Altiparmak D, Usta H. Development and testing of a prototype of absorption heat pump system operated by solar energy. Appl Therm Eng 2002;22:1847–59.
[61] Izquierdo M, Vega MD, Lcuona A, Rodriguez P. Compressors driven by thermal solar energy: entropy generated, exergy destroyed and exergetic efficiency. Sol Energy 2002;72(4):363–75.
[62] Anyanwu EE, Ogueke NV. Thermodynamic design procedure for solid adsorption solar refrigerator. Renew Energy 2005;30:81–96.
[63] Pons M, Meunier F, Cacciola G, Critoph RE, Groll M, Puigjaner L, et al. Thermodynamic based comparison of sorption systems for cooling and heat pumping. Int J Refrig 1999;22:5–17.
[64] Garcia-Rodriguez L, Gomez-Camacho C. Exergy analysis of the SOL-14 plant (Plataforma Solar de Almeria, Spain). Desalination 2001;137:251–8.
[65] You Y, Hu EJ. A medium-temperature solar thermal power system and its efficiency optimization. Appl Therm Eng 2002;22(4):357–64.
[66] Fujisawa T, Tani T. Annual exergy evaluation on photovoltaic-thermal hybrid collector. Sol Energy Mater Sol Cells 1997;47:135–48.
[67] Saitoh H, Hamada Y, Kubota H, Nakamura M, Ochifuji K, Yokoyama S, et al. Field experiments and analyses on a hybrid solar collector. Appl Therm Eng 2003;23:2089–105.
[68] Şahin AD, Dincer I, Rosen MA. Thermodynamic analysis of wind energy. Int J Energy Res 2006; 30(8):553–66.
[69] Ozgener O, Ozgener L. Exergy and reliability analysis of wind turbine systems: a case study. Renew Sustain Energy Rev 2006, in press, doi:10.1016/j.rser.2006.03.004.
[70] Lee KC. Classification of geothermal resources an engineering approach. In: Proceedings of 21st workshop on geothermal reservoir engineering, Stanford University; 1996. 5pp.
[71] Lee KC. Classification of geothermal resources by exergy. Geothermics 2001;30:431–42.
[72] Quijano J. Exergy analysis for the Ahuachapan and Berlin geothermal fields, El Salvador. In: Proceedings of world geothermal congress, Kyushu-Tohoku, Japan, 28 May–10 June 2000.
[73] Ozgener L, Hepbasli A, Dincer I. Thermo-mechanical exergy analysis of Balcova geothermal district heating system in Izmir, Turkey. ASME—J Energy Resour Technol 2004;126:293–301.
[74] Baba A, Ozgener L, Hepbasli A. Environmental and exergetic aspects of geothermal energy. Energy Sources 2006;28(7):597–609.
[75] Muffler P, Cataldi R. Methods of regional assessment of geothermal resources. Geothermics 1978;7:53–89.
[76] Benderitter Y, Cormy G. Possible approach to geothermal research and relative cost estimate. In: Dickson MH, Fanelli M, editors. Small geothermal resources. UNITAR/UNDP Centre for Small Energy Resources, Rome, Italy, 1990. p. 61–71.
[77] Hochstein MP. Classification and assessment of geothermal resources. In: Dickson MH, Fanelli M, editors. Small geothermal resources. UNITAR/UNDP Centre for Small Energy Resources, Rome, Italy, 1990. p. 31–59.
[78] Ozgener L, Hepbasli A, Dincer I. Energy and exergy analysis of the Gonen geothermal district heating system, "Turkey". Geothermics 2005;34:632–45.
[79] Ozgener L, Hepbasli A, Dincer I. Exergy analysis of Salihli geothermal district heating system in Manisa, Turkey. Int J Energy Res 2005;29(5):398–408.

[80] Etemoglu AB, Can M. Classification of geothermal resources in Turkey by exergy analysis. Renew Sustain Energy Rev 2006, in press, doi:10.1016/j.rser.2006.01.001.
[81] Ozgener L, Hepbasli A, Dincer I. Thermo-mechanical exergy analysis of Balcova geothermal district heating system in Izmir, Turkey. ASME—J Energy Resour Technol 2004;126:293–301.
[82] Ozgener L, Hepbasli A, Dincer I. Energy and exergy analysis of the Gonen geothermal district heating system in Turkey. Geothermics 2005;34(5):632–45.
[83] Ozgener L, Hepbasli A, Dincer I. Investigation of the energetic and exergetic performance of the Gonen geothermal district heating system. Proc Inst Mech Eng A J Power Energy 2006;220(7):671–9.
[84] Ozgener L, Hepbasli A, Dincer I, Rosen MA. Exergoeconomic modeling of geothermal district heating systems for building applications. In: Building simulation, Montreal, Canada, 15–18 August 2005.
[85] Ozgener L, Hepbasli A, Dincer I. Thermodynamic analysis of a geothermal district heating system. Int J Exergy 2005;2(3):231–45.
[86] Ozgener L, Hepbasli A, Dincer I. Parametric study of the effect of reference state on energy and exergy efficiencies of geothermal district heating systems (GDHSs): an application of the Salihli GDHS in Turkey. Heat Transfer Eng (2007, in press).
[87] Ozgener L, Hepbasli A, Dincer I. Effect of reference state on the performance of energy and exergy evaluation of geothermal district heating systems: Balcova example. Build Environ 2006;41(6):699–709.
[88] Ozgener L, Hepbasli A, Dincer I. A key review on performance improvement aspects of geothermal district heating systems and applications. Renew Sustain Energy Rev 2006, in press, doi:10.1016/j.rser.2006.03.006.
[89] Dincer I, Hepbasli A, Ozgener L. Geothermal energy resources. Encyclopedia of Energy Engineering. Marcel Dekker, 2007.
[90] Ozgener L, Hepbasli A, Dincer I. Energy and exergy analysis of Salihli geothermal district heating system in Manisa. Turkey. Int J Energy Res 2005;29:393–408.
[91] Ozgener L, Hepbasli A, Dincer I. Energy and exergy analysis of geothermal district heating systems: an application. Build Environ 2005;40(10):1309–22.
[92] Hepbasli A. Ground-source heat pumps. In: Cutler J, Cleveland CJ, editor-in-chief. The encyclopedia of energy. vol. 3. Academic Press/Elsevier Inc.: USA; 2004. p. 97–106.
[93] Hepbasli A. Thermodynamic analysis of a ground-source heat pump system for district heating. Int J Energy Res 2005;7:671–87.
[94] Ozgener O, Hepbasli A. Experimental performance analysis of a solar assisted ground-source heat pump greenhouse heating system. Energy Build 2005;37:101–10.
[95] Hepbasli A, Akdemir O. Energy and exergy analysis of a ground source (geothermal) heat pump system. Energy Convers Manage 2004;45:737–53.
[96] Ozgener O, Hepbasli A. A parametrical study on the energetic and exergetic assessment of a solar assisted vertical ground-source heat pump system used for heating a greenhouse. Build Environ 2006, in press, doi:10.1016/j. 2007;42(1):11–24.
[97] Akpinar EK, Hepbasli A. A comparative study on exergetic assessment of two ground-source (geothermal) heat pump systems for residential applications. Build Environ 2006, in press, doi:10.1016/j.buildenv.2006.04.001.
[98] Crawford RR. An experimental laboratory investigation of second law analysis of a vapor-compression heat pump. ASHRAE Trans 1988;94(2):1491–504.
[99] Salah El-Din MM. Optimization of totally irreversible refrigerators and heat pumps. Energy Convers Manage 1999;40:423–36.
[100] Hepbasli A, Dincer I, Rosen MA. Exergy analysis of heat pump systems for residential applications. In: CD-Proceedings of seventh international HVAC + R technology symposium, Istanbul, Turkey, 8–10 May 2006.
[101] Hepbasli A, Ozgener O. Performance evaluation of ground-source (geothermal) heat pump systems using exergy analysis method. In: CD-Proceedings of CLIMA-2005 conference, Lousanne, Switzerland, 9–12 October 2005.
[102] Ozgener O, Hepbasli A, Dincer I. Performance improvement of ground-source heat pump systems (GSHPSs) for Residential applications. In: CD-Proceedings of second international exergy, energy and environent symposium (IEEES-2), Kos, Greece, 3–7 July 2005.
[103] Ozgener O, Hepbasli A. Modeling and performance evaluation of ground source (geothermal) heat pump systems. Energy Build 2007;39(1):66–75.
[104] Ozgener O, Hepbasli A. Exergoeconomic analysis of a solar assisted ground-source heat pump greenhouse heating system. Appl Therm Eng 2005;25:1459–71.

[105] Ozgener O, Hepbasli A. A review on the energy and exergy analysis of solar assisted heat pump systems. Renew Sustain Energy Rev 2007;11(3):482–96.
[106] Kara YA. Utilization of low temperature geothermal resources for space heating by using GHPs. Ph.D. thesis, Ataturk University, Erzurum, Turkey, 1999. p. 130 (in Turkish).
[107] Kara YA, Yuksel B. Evaluation of low temperature geothermal energy through the use of heat pump. Energy Convers Manage 2000;42:773–81.
[108] Midilli A, Kucuk H. Energy and exergy analysis of solar drying process of pistachio. Energy 2003;28:539–56.
[109] Dincer I, Sahin AZ. A new model for thermodynamic analysis of a drying process. Int J Heat Mass Transfer 2004;47:645–52.
[110] Akpinar EK. Energy and exergy analyses of drying of red pepper slices in a convective type dryer. Int Commun Heat Mass Transfer 2004;31(8):1165–76.
[111] Akpinar EK, Midilli A, Bicer Y. Energy and exergy of potato drying process via cyclone type dryer. Energy Convers Manage 2005;46(15&16):2530–52.
[112] Akpinar EK, Midilli A, Bicer Y. The first and second law analyses of thermodynamic of pumpkin drying process. J Food Eng 2006;72(4):320–31.
[113] Syahrul S, Hamdullahpur F, Diner I. Exergy analysis of fluidized bed drying of moist particles. Exergy Int J 2002;2:87–98.
[114] Akpinar EK, Midilli A, Bicer Y. Thermodynamic analysis of the apple drying process. Proc IMechE Part E: J Process Mech Eng 2005;219:1–14.
[115] Kuzgunkaya EH, Hepbasli A. Exergetic evaluation of drying of laurel leaves in a vertical ground-source heat pump drying cabinet. Int J Energy Res (2006, in press).
[116] DiPippo R. Small geothermal power plants: design, performance and economics. GHC Bull 1999;June:1–8.
[117] Badvarsson G, Eggers DE. The exergy of thermal water. Geothermics 1972;1:93–5.
[118] DiPippo R. Second law analysis of flash-binary and multilevel binary geothermal power plants. Geotherm Resour Council Trans 1994;18:505–10.
[119] Kanoglu M. Exergy analysis of a dual-level binary geothermal power plant. Geothermics 2004;31:709–24.
[120] DiPippo R. Second Law assessment of binary plants generating power from low-temperature geothermal fluids. Geothermics 2004;33:565–86.
[121] Dagdas A, Ozturk R, Bekdemir S. Thermodynamic evaluation of Denizli Kızıldere geothermal power plant and its performance improvement. Energy Convers Manage 2005;46:245–56.
[122] Ozturk HK, Atalay O, Yilan A, Hepbasli A. Energy and exergy analysis of Kizildere geothermal power plants, Turkey. Energy Sources A 2006;28(15):1415–24.
[123] Cerci Y. Performance evaluation of a single-flash geothermal power plant in Denizli, Turkey. Energy 2003;28:27–35.
[124] Yildirim ED, Gokcen G. Exergy analysis and performance evaluation of Kizildere geothermal power plant, Turkey. Int J Exergy 2004;1(3):316–33.
[125] Setiawan B. Exergy analysis and performance evaluation of Salak geothermal power plant, Indonesia, Project Report, No: GEOTHERM 96.24, Geothermal Institute, The University of Auckland, New Zealand, 1996.
[126] Koreneos C, Bobolias C, Spachos T. Evaluation of utilization opportunities of geothermal energy in the Kavala region, Greece, using exergy analysis. Int J Exergy 2004;1(1):111–27.
[127] Dagdas A, Erdem HH, Sevilgen SH. Performance analysis of gas turbine integrated geothermal power plant in Turkey: the proposed Kizildere project. In: CD-Proceedings of world geothermal congress 2005, Antalya, Turkey, 24–29 April 2005.
[128] Govin OV, Diky OV, Kabo GJ, Blokhin AV. Evaluation of the chemical exergy of fuels and petroleum fractions. J Therm Anal Calorimetry 2000;62:123–33.
[129] Hepbasli A, Ozgener L, Ozgener O. Comparison of energy and exergy prices of various energy sources for the residential use. In: CD-Proceedings of seventh international HVAC+R technology symposium, Istanbul, Turkey, 8–10 May 2006.
[130] Nilsson D. Energy, exergy and emergy analysis of using straw as fuel in district heating plants. Biomass Bioenergy 1997;13(l/2):63–73.
[131] Zhong C, Peters CJ, de Swaan Aron J. Thermodynamic modeling of biomass conversion processes. Fluid Phase Equilibria 2002;194–197:805–15.
[132] Panopoulos KD, Fryda L, Karl J, Poulou S, Kakaras E. High temperature solid oxide fuel cell integrated with novel allothermal biomass gasification: Part II: Exergy analysis. J Power Sources 2006;159(1):586–94.

[133] Franco A, Giannini N. Perspectives for the use of biomass as fuel in combined cycle power plants. Int J Thermal Sci 2005;44:163–77.
[134] Shieh JH, Fan LT. Estimation of energy (enthalpy) and exergy (availability) contents in structurally complicated materials. Energy Sources 1982;6:1–45.
[135] Raoa MS, Singh SP, Sodhaa MS, Dubeyb AK, Shyamb M. Stoichiometric, mass, energy and exergy balance analysis of countercurrent fixed-bed gasification of post-consumer residues. Biomass Bioenergy 2004;27:155–71.
[136] Bilgen S, Kaygusuz K, Sari A. Second law analysis of various types of coal and woody biomass in Turkey. Energy Sources 2004;26:1083–94.
[137] Srivastava A. Second law (exergy) analysis of various types of coal. Energy Convers Manage 1988;28: 117–21.
[138] Bejan A, Tsatsaronis G, Moran M. Thermal design and optimisation. New York: Wiley; 1996.
[139] Utlu Z, Hepbasli A, Akdeniz RC. Exergetic assessment of cotton stalk production in the Turkish agricultural sector. In: Proceedings of the ninth international congress on mechanization and energy in agriculture & 27th international conference of CIGR Section IV: The Efficient Use of Electricity and Renewable Energy Sources in Agriculture, September 27–29, İzmir, Turkey, 2005. p. 231–9.
[140] Prins MJ, Ptasinski KJ, Janssen FJJG. More efficient biomass gasification via torrefaction. Energy 2006;31(15):3458–70.
[141] Ozger M, Altunkaynak A, Sen Z. Statistical investigation of expected wave energy and its reliability. Energy Convers Manage 2004;45(13&14):2173–85.
[142] Tucker MJ, Pitt EG. Waves in ocean engineering. Oxford: Elsevier Science; 2001.
[143] Wark JK. Advanced thermodynamics for engineers. New York: McGraw-Hill Companies Inc.; 1995.
[144] Ertesvag IS. Society exergy analysis: a comparison of different societies. Energy 2001;26:253–70.
[145] Utlu Z, Hepbasli A. A review on analyzing and evaluating the energy utilization efficiency of countries. Renew Sustain Energy Rev 2007;11(1):1–29.
[146] Milia D, Sciubba E. Exergy-based lumped simulation of complex systems: an interactive analysis tool. In: Venere P, editor. Proceedings of the second international workshop on advanced energy studies, Italy; 2000. p. 513–23.
[147] Ertesvåg IS. Energy, exergy, and extended-exergy analysis of the Norwegian society 2000. Energy 2005(30):645–79.
[148] Hepbasli A, Utlu Z. Analyzing the energy utilization efficiency of renewable energy resources. Part 2: exergy analysis method. Energy Sources B: Econ Planning Policy 2006;1(4), in press.
[149] Dincer I, Hussain MM, Al-Zaharnah I. Energy and exergy utilization in transportation sector of Saudi Arabia. Appl Therm Eng 2004;24:525–38.
[150] Dincer I, Hussain MM, Al-Zaharnah I. Analysis of sectoral energy and exergy use of Saudi Arabia. Int J Energy Res 2004;28:205–43.
[151] Unal A. Energy and exergy balance for Turkey in 1991. MSc thesis, University of Middle East Technical University, Ankara, Turkey, 1994.
[152] Rosen MA, Dincer I. Sectoral energy and exergy modeling of Turkey. Trans ASME 1997;119:200–4.
[153] Ileri A, Gurer T. Energy and exergy utilization in Turkey during 1995. Energy 1998;23(12):1099–106.
[154] Utlu Z, Hepbasli A. Turkey's sectoral energy and exergy analysis between 1999 and 2000. Int J Energy Res 2004;28:1177–96.